TECHNICAL REPORT HL-81-12

EVALUATION OF IN-RESERVOIR COFFERDAM ON RICHARD B. RUSSELL RESERVOIR AND HYDROPOWER RELEASES

Hybrid Model Investigation

by

Dennis R. Smith, Jeffrey P. Holland, Bruce Loftis, Charles H. Tate, Jr.

Hydraulics Laboratory
U. S. Army Engineer Waterways Experiment Station
P. O. Box 631, Vicksburg, Miss. 39180

October 1981

Final Report

Approved For Public Release; Distribution Unlimited

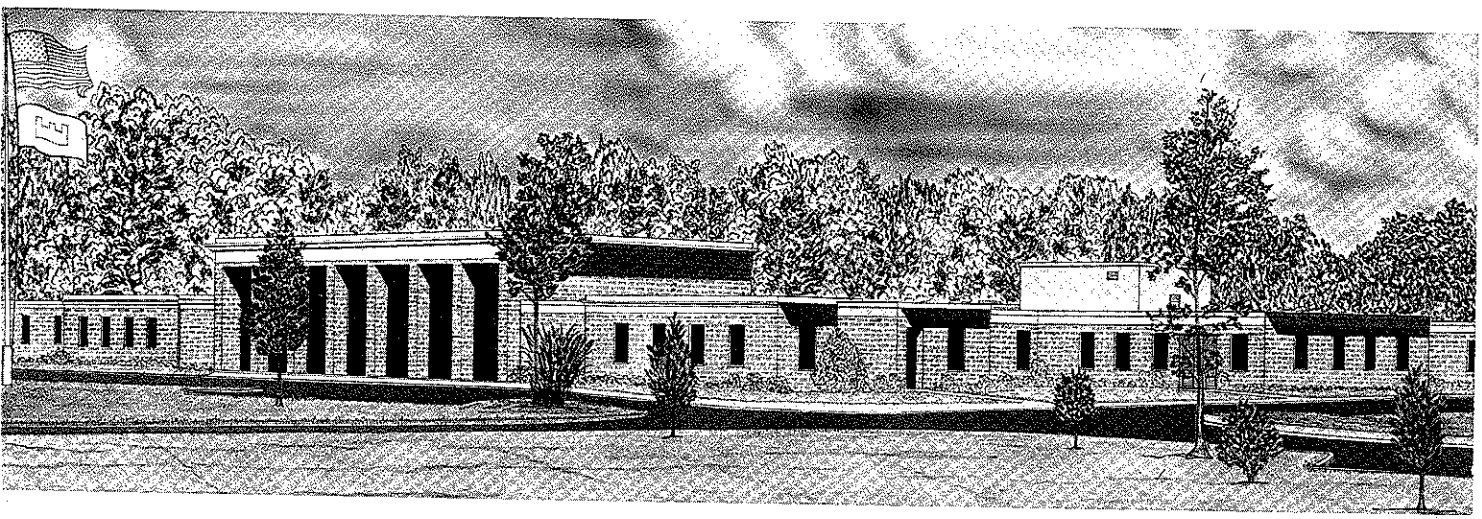

Prepared for U. S. Army Engineer District, Savannah
Savannah, Georgia 31402

Destroy this report when no longer needed. Do not return it to the originator.

The findings in this report are not to be construed as an official Department of the Army position unless so designated by other authorized documents.

The contents of this report are not to be used for advertising, publication, or promotional purposes. Citation of trade names does not constitute an official endorsement or approval of the use of such commercial products.

REPORT DOCUMENTATION PAGE

READ INSTRUCTIONS BEFORE COMPLETING FORM

1. REPORT NUMBER: Technical Report HL-81-12
2. GOVT ACCESSION NO.:
3. RECIPIENT'S CATALOG NUMBER:

4. TITLE (and Subtitle): EVALUATION OF IN-RESERVOIR COFFERDAM ON RICHARD B. RUSSELL RESERVOIR AND HYDROPOWER RELEASES; Hybrid Model Investigation

5. TYPE OF REPORT & PERIOD COVERED: Final report

6. PERFORMING ORG. REPORT NUMBER:

7. AUTHOR(s): Dennis R. Smith, Jeffrey P. Holland, Bruce Loftis, Charles H. Tate, Jr.

8. CONTRACT OR GRANT NUMBER(s):

9. PERFORMING ORGANIZATION NAME AND ADDRESS
U. S. Army Engineer Waterways Experiment Station
Hydraulics Laboratory
P. O. Box 631, Vicksburg, Miss. 39180

10. PROGRAM ELEMENT, PROJECT, TASK AREA & WORK UNIT NUMBERS:

11. CONTROLLING OFFICE NAME AND ADDRESS
U. S. Army Engineer District, Savannah
P. O. Box 889
Savannah, Ga. 31402

12. REPORT DATE: October 1981

13. NUMBER OF PAGES: 55

14. MONITORING AGENCY NAME & ADDRESS(if different from Controlling Office):

15. SECURITY CLASS. (of this report): Unclassified

15a. DECLASSIFICATION/DOWNGRADING SCHEDULE:

16. DISTRIBUTION STATEMENT (of this Report)

Approved for public release; distribution unlimited.

17. DISTRIBUTION STATEMENT (of the abstract entered in Block 20, if different from Report)

18. SUPPLEMENTARY NOTES

Available from National Information Technical Service, 5285 Port Royal Road, Springfield, Va. 22151.

19. KEY WORDS (Continue on reverse side if necessary and identify by block number)

Pumped storage
Stratified flow characteristics
Hydrodynamics
Physical modeling
Mathematical modeling

20. ABSTRACT (Continue on reverse side if necessary and identify by block number)

The U. S. Army Corps of Engineers, Savannah District, will install an innovative oxygen injection system in the proposed Richard B. Russell Reservoir to enhance the dissolved oxygen distribution in the reservoir and in the release. To complement this effort, a hybrid modeling study was conducted to evaluate the compatibility of various in-reservoir geometries with the injection scheme. The relative impact of four in-reservoir geometries upon the in situ and release water quality was investigated. Additionally, idealized

(Continued)

20. ABSTRACT (Continued).

calculations were made to determine the respective injection rates required to maintain a release dissolved oxygen concentration of 6 mg/ℓ (or more).

PREFACE

The hybrid model (combination of physical and numerical models) investigation reported herein was authorized by the U. S. Army Engineer District, Savannah, and conducted during the period January 1978-January 1980 in the Hydraulics Laboratory of the U. S. Army Engineer Waterways Experiment Station (WES) under the direction of Messrs. H. B. Simmons, Chief of the Hydraulics Laboratory, John L. Grace, Jr., Chief of the Hydraulic Structures Division, and Dr. Dennis R. Smith, Chief of the Reservoir Water Quality Branch. The physical model studies were conducted by Mr. Charles H. Tate, Jr., with assistance from Messrs. Alvin Myers, Calvin Buie, Jr., and Ms. Sadie Redmond. The numerical simulations and analyses were conducted by Messrs. Bruce Loftis and Jeffrey P. Holland with assistance from Ms. Mary K. McElroy and Mr. Terry W. Reeves. This report was prepared by Dr. Smith, Messrs. Holland, Loftis, and Tate. Messrs. Jim Gallagher, Gary Mauldin, and Randy Miller served as point of contact within Savannah District.

Commanders and Directors of WES during the conduct of this study and the preparation and publication of the report were COL John L. Cannon, CE, COL Nelson P. Conover, CE, and COL Tilford C. Creel, CE. Technical Director was Mr. F. R. Brown.

CONTENTS

CONVERSION FACTORS, U. S. CUSTOMARY TO METRIC (SI)
UNITS OF MEASUREMENT

U. S. customary units of measurement used in this report can be converted to metric (SI) units as follows:

Multiply	By	To Obtain
acres	4046.856	square metres
acre-feet	1233.482	cubic metres
Btu (International Table)	1055.056	joules
Btu (International Table)/ lb/°F	4186.800	joules per kilogram kelvin
cubic feet per second	0.02831685	cubic metres per second
Fahrenheit degrees	5/9	Celsius degrees or Kelvins*
feet	0.3048	metres
feet per second per second	0.3048	metres per second per second
miles (U. S. statute)	1.609344	kilometres
pounds (mass) per cubic foot	16.01846	kilograms per cubic metre
square feet	0.09290304	square metres
tons (2,000 lb, mass)	907.1847	kilograms

* To obtain Celsius (C) temperature readings from Fahrenheit (F) readings, use the following formula: $C = (5/9)(F - 32)$. To obtain Kelvin (K) readings, use: $K = (5/9)(F - 32) + 273.15$.

EVALUATION OF IN-RESERVOIR COFFERDAM ON RICHARD B. RUSSELL RESERVOIR AND HYDROPOWER RELEASES

Hybrid Model Investigation

PART I: BACKGROUND

1. A coldwater release (less than 70°F)* with a dissolved oxygen (D.O.) concentration of 6 mg/ℓ is desired from the proposed Richard B. Russell Reservoir (RBRR) and pumped storage hydropower facilities. During stratification of the reservoir, the respective vertical distributions of temperature and D.O. essentially preclude withdrawal and release of water that meets both objectives. If sufficient epilimnetic water is withdrawn to meet the D.O. objective, the upper bound of the temperature criterion is exceeded. Conversely, if adequate cold hypolimnetic water is withdrawn to meet the temperature objective, the withdrawn D.O. concentration is less than that desired; thus, if adequate reaeration does not occur in or below the hydropower structure, the D.O. objective will not be met. To circumvent this potential problem, the U. S. Army Engineer District, Savannah (SAS) will (a) place the center line of the hydropower intakes approximately 70 ft below the surface of the pool to withdraw cold water and (b) install an innovative oxygenation system in RBRR to increase the D.O. concentration in the withdrawal zone of the reservoir. Obviously, large quantities of molecular oxygen are involved in this procedure. As a result, SAS and the U. S. Army Engineer Division, South Atlantic (SAD), requested the U. S. Army Engineer Waterways Experiment Station (WES) to investigate the relative effectiveness and/or feasibility of various in-reservoir structural alternatives in enhancing the in situ D.O. in the reservoir withdrawal zone, thus reducing the quantity (or rate) of oxygen required for injection. The in-reservoir design options identified by SAS and SAD were:

---

* A table of factors for converting U. S. customary units of measurement to metric (SI) units is presented on page 3.

a. Option A: removal of the cofferdam (as originally planned).

b. Option B: continuous cofferdam as-constructed with a crest at el 378.* Diversion breach would be filled.

c. Option C: cofferdam left in place as-constructed and without filling the second stage 50-ft-long diversion breach (bottom at el 310).

d. Option D: a sheet-pile cutoff wall installed on the crest of the continuous cofferdam with the top at el 400.

A schematic of the geometries is presented in Figure 1.

Project Description

2. The RBRR is a multipurpose project currently nearing completion of construction by SAS. The project, which will impound the Savannah River between the headwaters of Clarks Hill Reservoir and Hartwell Dam (Figure 2), is designed to provide hydropower. The dam consists of a 195-ft-high, 1884-ft-long concrete gravity structure flanked by two earth embankments. The powerhouse will house four 75-MW conventional units and four 75-MW pump units. Total capacity of the system is 600 MW. Withdrawal for these units will be accomplished through eight penstocks; each penstock has a cross-section area of approximately 5400 ft and is located at center-line el 393.

3. The RBRR will have a surface area of 26,650 acres when filled to maximum power pool, el 475. At this elevation the reservoir will have a storage volume of approximately 1,026,200 acre-ft and will extend up the Savannah River to the vicinity of the Hartwell Dam. Depth of the reservoir at maximum power pool will be 165.0 ft. The release of excessive flood flows will be accomplished by a 500-ft-long ogee spillway.

Approach

4. The hybrid modeling approach was used in this study. A

* All elevations (el) cited herein are in feet referred to mean sea level (msl).

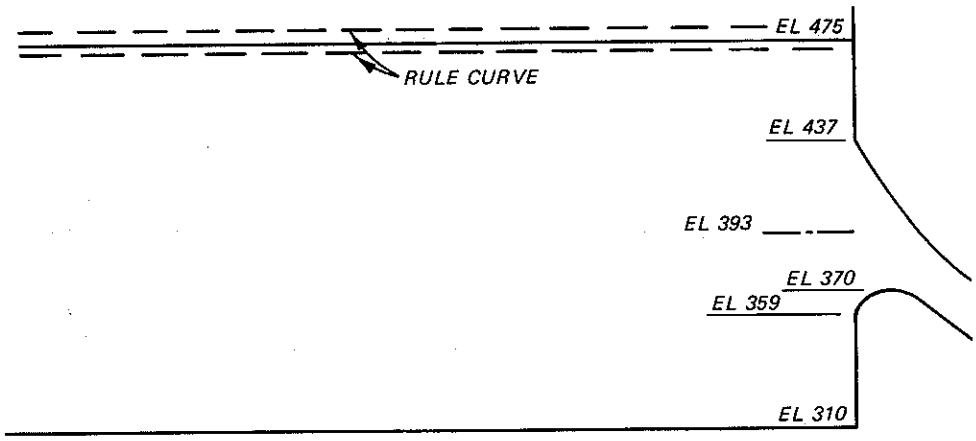

a. Cofferdam removed, Option A

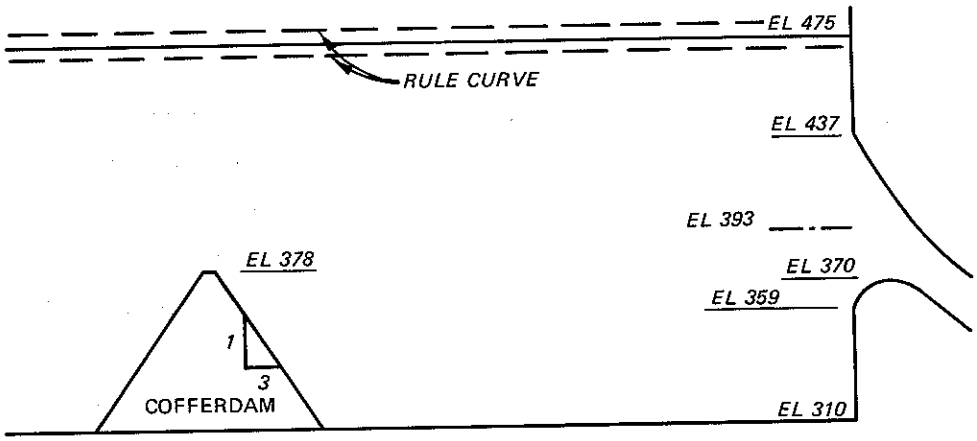

b. Continuous or breached cofferdam (Options B and C)

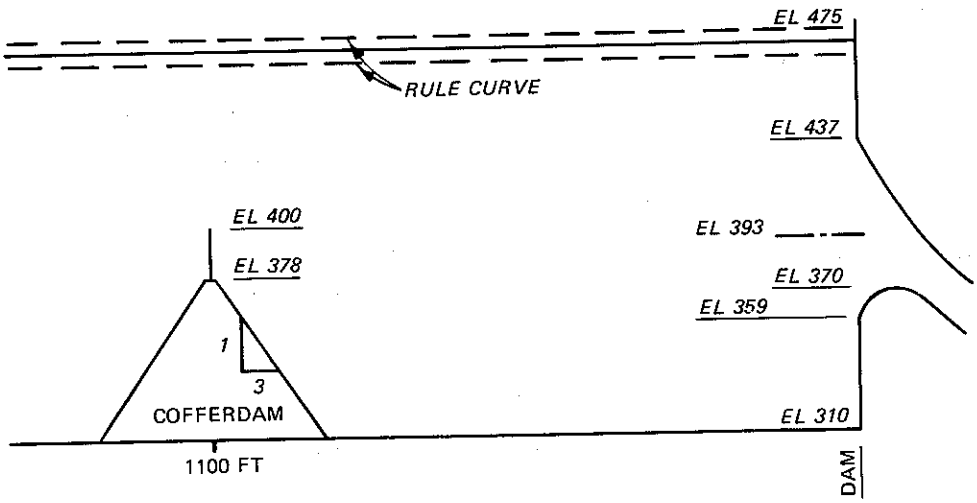

c. Raised cofferdam, Option D

Figure 1. Schematic of in-reservoir geometrical alternatives

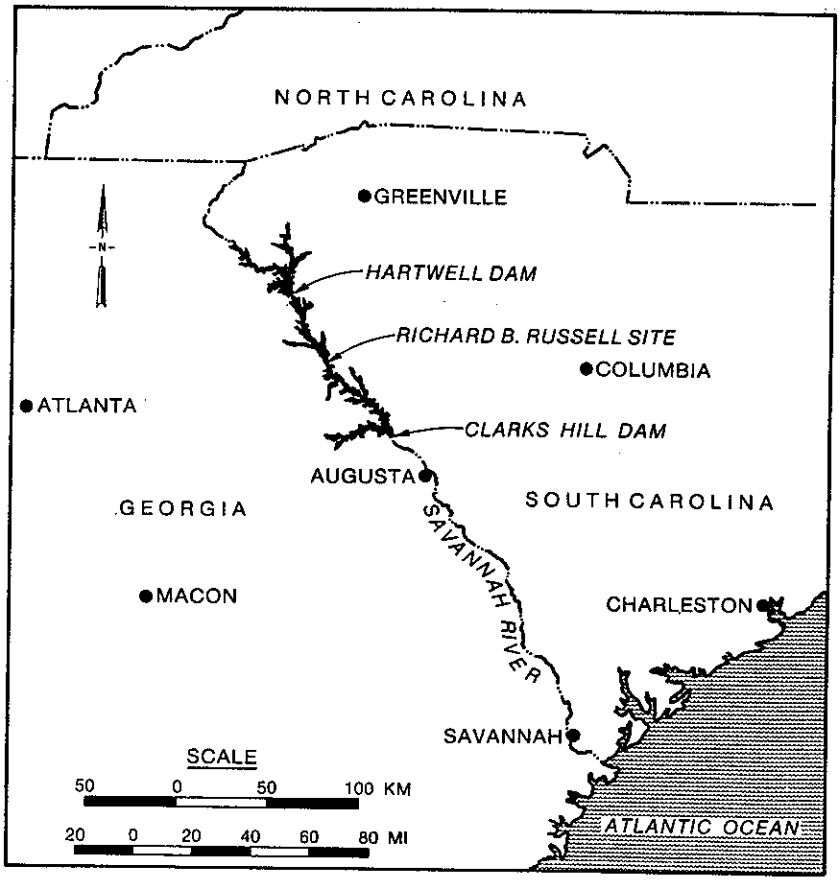

Figure 2. Location map

numerical simulation model, WESTEX, was adopted from previous analyses of pumped storage projects.* Details of the numerical model are provided in Appendix A. Algorithms that addressed the selective-withdrawal and pumpback processes were developed and calibrated with data obtained from an undistorted-scale physical model that simulated the hydrodynamics occurring near the dam. The physical model was constructed to a 1:150 scale and reproduced the dam and approximately 3000 ft of the upstream

* M. S. Dortch el al. 1976 (Dec). "Dickey-Lincoln School Lakes Hydrothermal Model Study; Hydraulic Model Investigation," Technical Report H-76-22, U. S. Army Engineer Waterways Experiment Station, CE, Vicksburg, Miss.
D. G. Fontane et al. 1977 (Apr). "Marysville Lake Hydrothermal Study: 900-MW Project; Hydraulic and Mathematical Model Investigation," Technical Report H-77-5, Report 1, U. S. Army Engineer Waterways Experiment Station, CE, Vicksburg, Miss.

topography. Additional details of the physical model and the selective withdrawal and the pumpback descriptions developed from the model data are provided in Appendix B. The numerical model was used with historical hydrology and meteorology for 1955, 1958, 1966, and 1967 to simulate the reservoir temperature and vertical distributions of D.O. and the release temperature and D.O. concentrations expected during the four study years with each of the in-reservoir design alternatives. The respective predictions for each in-reservoir design alternative were then compared to ascertain their relative merits in enhancing the D.O. distribution in the reservoir and the D.O. concentration in the release.

PART II: ACQUISITION AND DEVELOPMENT OF DATA

5. The simulation model (WESTEX) required data for lake inflows, outflows, inflow stream temperature, various meteorological data, and a schedule reflecting daily power (generation and pumpback) operations. The WESTEX model also required determination of coefficients for surface heat exchange and for internal mixing. Various data required by the simulation model are described below.

Meteorology

6. Meteorological data for the Atlanta, Georgia, Class A weather station was obtained from the National Climatic Center, Asheville, North Carolina. The required data consisted of dry bulb and dewpoint temperatures, wind speed, and cloud cover. From these data, daily average values of equilibrium temperature, surface heat exchange coefficient, and net solar radiation quantity were computed. For each study year, these parameters were computed by the U. S. Army Engineer Division, Ohio River.

Lake Geometry

7. The elevation-capacity data for RBRR and the location and design of the penstocks were supplied by SAS.

Inflow Quantity and Temperature

8. Both the inflow quantities and temperature were obtained from observed outflow quantities and temperatures from Hartwell Dam, which will release directly into RBRR. These values were supplied by SAS.

Power Operations

9. Conventional power generation releases at RBRR will range from

0 to 35,000 cfs during a one-day period. Pumped storage operations at RBRR will increase the upper bound of the hydropower releases to 60,000 cfs. The proposed operation schedule indicates that the pumpback rates from the headwaters of Clarks Hill to RBRR will remain nearly constant at 20,000 cfs. The load curve used by Fontane and Bohan* appears in Figure 3 and was used for this study as directed by SAS. For each simulation day, a schedule of operations representing one or two generation cycles and one (or none, if conventional power only) pumpback cycle was modeled after Figure 3. The number of hours of generation was held constant for each day as shown in the load curve. The generation release rates matched the outflow data supplied by SAS.

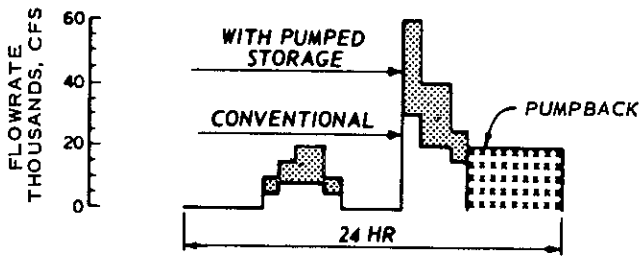

Figure 3. RBRR load curve

Coefficient Selection

10. As has been discussed previously, the WESTEX model requires determination of coefficients of surface heat exchange and internal mixing. Two surface heat exchange coefficients must be selected: β, the shortwave radiation absorbed in the surface layer, and λ, the light extinction coefficient. Similarly, two mixing coefficients, α_1 and α_2, must be selected. These coefficients are analogous to mixing produced by vertical diffusion. The four coefficients were predicated upon a comparison of predicted profiles for RBRR without pumpback with observed profiles from Hartwell Reservoir. Hartwell Reservoir is

* D. G. Fontane and J. P. Bohan. 1974 (Dec). "Richard B. Russell Lake Water Quality Investigation; Hydraulic Laboratory Investigation," Technical Report H-74-14, U. S. Army Engineer Waterways Experiment Station, CE, Vicksburg, Miss.

immediately upstream of RBRR and is similar in size. Additionally, Hartwell is subject to similar meteorological and hydrological conditions. The selected coeffecients were:

$\beta = 0.45$

$\lambda = 0.2$

$\alpha_1 = 0.15$

$\alpha_2 = 0.30$

PART III: RESULTS

11. The relative impact of the respective geometrical configurations upon the in-reservoir and release water quality can be demonstrated by comparing representative in situ and release water quality predictions. The in-reservoir results will be discussed first.

In-Reservoir Dissolved Oxygen and Temperature

Dissolved oxygen

12. Predicted D.O. profiles for the respective in-reservoir geometries are presented in Figures 4 and 5. Although these profiles are for only 27 September of the various study years, they are indicative of the relative effects that each geometry has upon the D.O. distribution during the late phases of stratification. As indicated in Figures 4 and 5, the most favorable D.O. distribution during the late phases of stratification is obtained if the cofferdam is removed (Option A, Figure 1). With the cofferdam removed, a larger volume of water is entrained from the hypolimnion into the pumpback jet. After entrainment, the low D.O. hypolimnetic water mixes with metalimnetic (or epilimnetic) waters. Simultaneously, water with higher D.O. from the epilimnion (or metalimnion) moves downward. Since oxygen is continually supplied to the epilimnion through the air-water interface, and since the volume from the hypolimnion pumped during a pumpback operation is small compared with the total volume of the epilimnion or metalimnion, significant D.O. depletion in the upper region does not occur. The continual supply of high D.O. water and the redistribution of this water results in a tendency to improve the D.O. distribution in the reservoir.

13. Any horizontal obstruction in the reservoir that reduces the quantity of water removed from the hypolimnion by entrainment will tend to decrease vertical mixing during pumpback. With the continuous and breached cofferdams (Options B and C, Figure 1), the physical model indicated 13 percent less entrainment from the hypolimnion than would occur if the cofferdam were removed. Thus, a less favorable D.O.

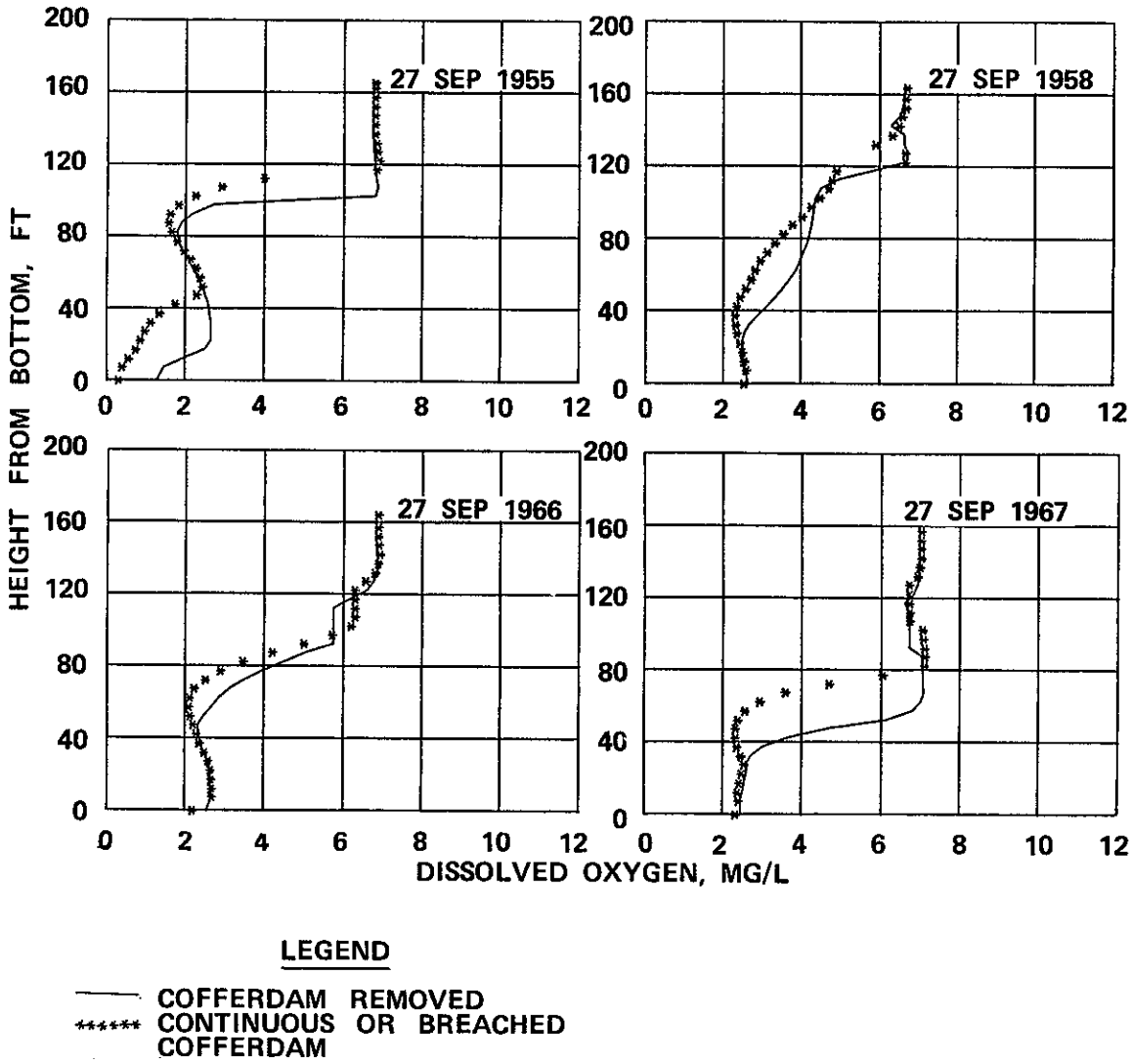

Figure 4. Predicted D.O. distribution without the cofferdam and with the continuous or breached cofferdam

distribution develops in the reservoir during the late phases of stratification (Figure 4) with the cofferdam than with its removal.

14. The numerical simulations for the breached cofferdam (Option C, Figure 1) were basically identical to the results obtained for the continuous cofferdam (Option B, Figure 1). This similarity occurred because the breach is small compared with the length of the dam and the area available for flow above the cofferdam. Although not simulated in the mathematical model, qualitative observations of physical simulations

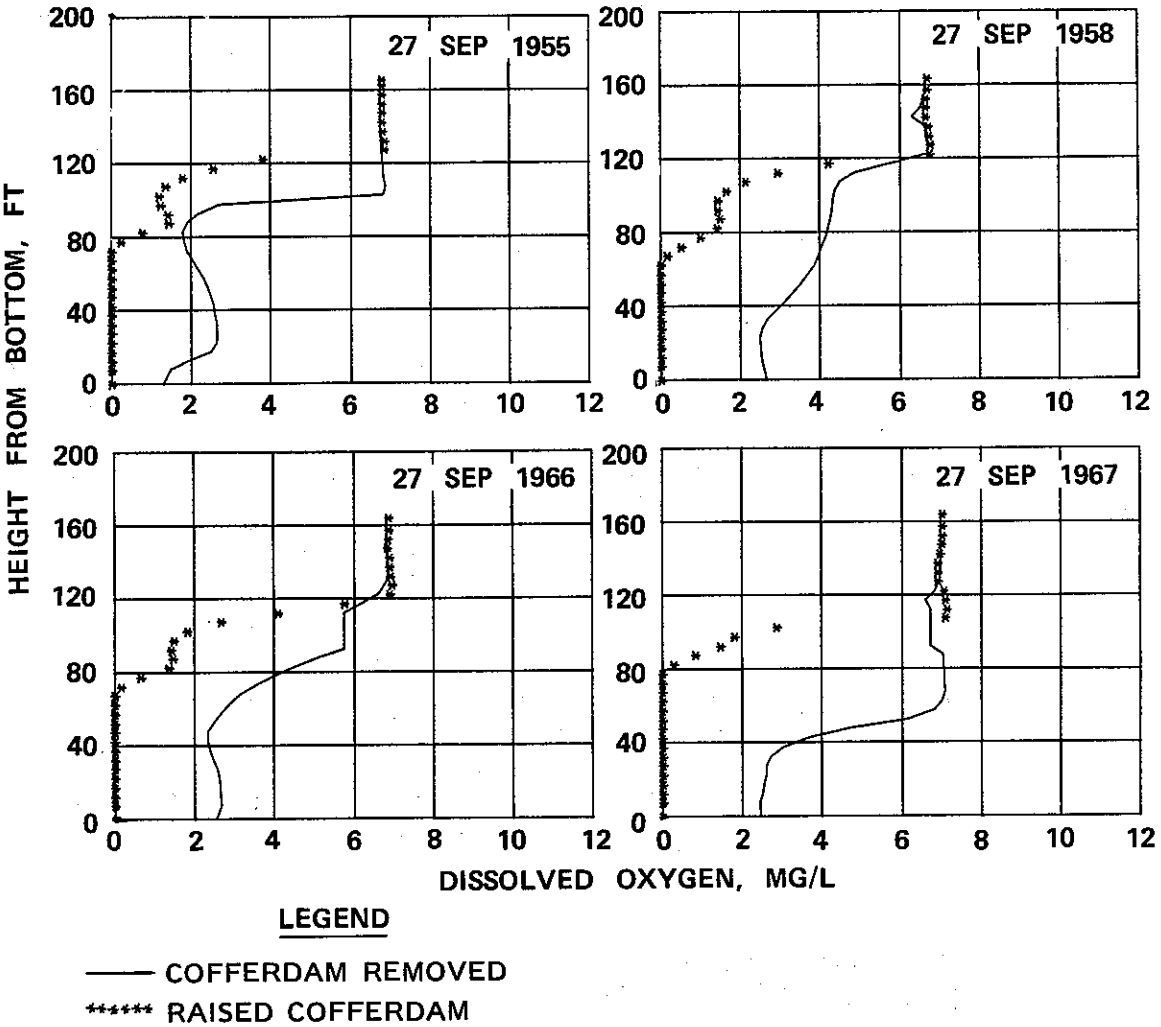

Figure 5. Predicted D.O. distribution with the cofferdam removed and with the raised cofferdam

indicated transient flow through the breach between pumpback and withdrawal phases. As a result, if the cofferdam is breached and poor water quality exists in the lower layers, gravity flow through the breach during the time interval between pumpback and release could result in poor water quality between the dam and the cofferdam. During subsequent hydropower release, a pulse of low D.O. water could occur.

15. Placing a sheet-pile cutoff wall with a crest at el 400 (Option D, Figure 1) severely mitigates vertical mixing during pumpback.

As compared with removal of the cofferdam (Option A), 90 percent less entrainment from the hypolimnion was measured in the physical model with the raised cofferdam. Depending upon the simulation year, anaerobic conditions developed in the hypolimnion in late June to mid-July. By the end of September, the thickness of the anaerobic zone had increased to between 65 and 80 ft depending upon the simulation year. As a result, this alternative is not considered viable and will not receive further consideration.

16. A synopsis of the in-reservoir analysis with respect to the D.O. distribution is presented in Table 1.

In-reservoir temperature

17. Representative temperature profiles are presented in Figure 6. Temperature distributions produced in the reservoir by withdrawal over the cofferdam were colder than those predicted with the cofferdam removed. The withdrawal distribution is higher in the reservoir as a result of withdrawal over the cofferdam which results in the release of warmer water and the retention of colder water.

Release Dissolved Oxygen

18. The predicted release D.O. concentration as a function of time for the 1966 and 1967 study years is presented in Figure 7. These results are similar to the results obtained for the 1955 and 1958 study years and may be used to demonstrate general findings.

Qualitative observations

19. Prior to June and after September (or October for conditions similar to 1955), the predicted release D.O. concentrations with the respective cofferdam geometries were essentially equivalent. The difference in the release D.O. for the respective geometries during these periods was less than 0.25 mg/ℓ. Thus, if the reservoir was unstratified or only weakly stratified, the in-reservoir geometry did not significantly impact the release D.O.

20. The release D.O. concentration was more sensitive to the in-reservoir geometry during significant stratification. In general, the

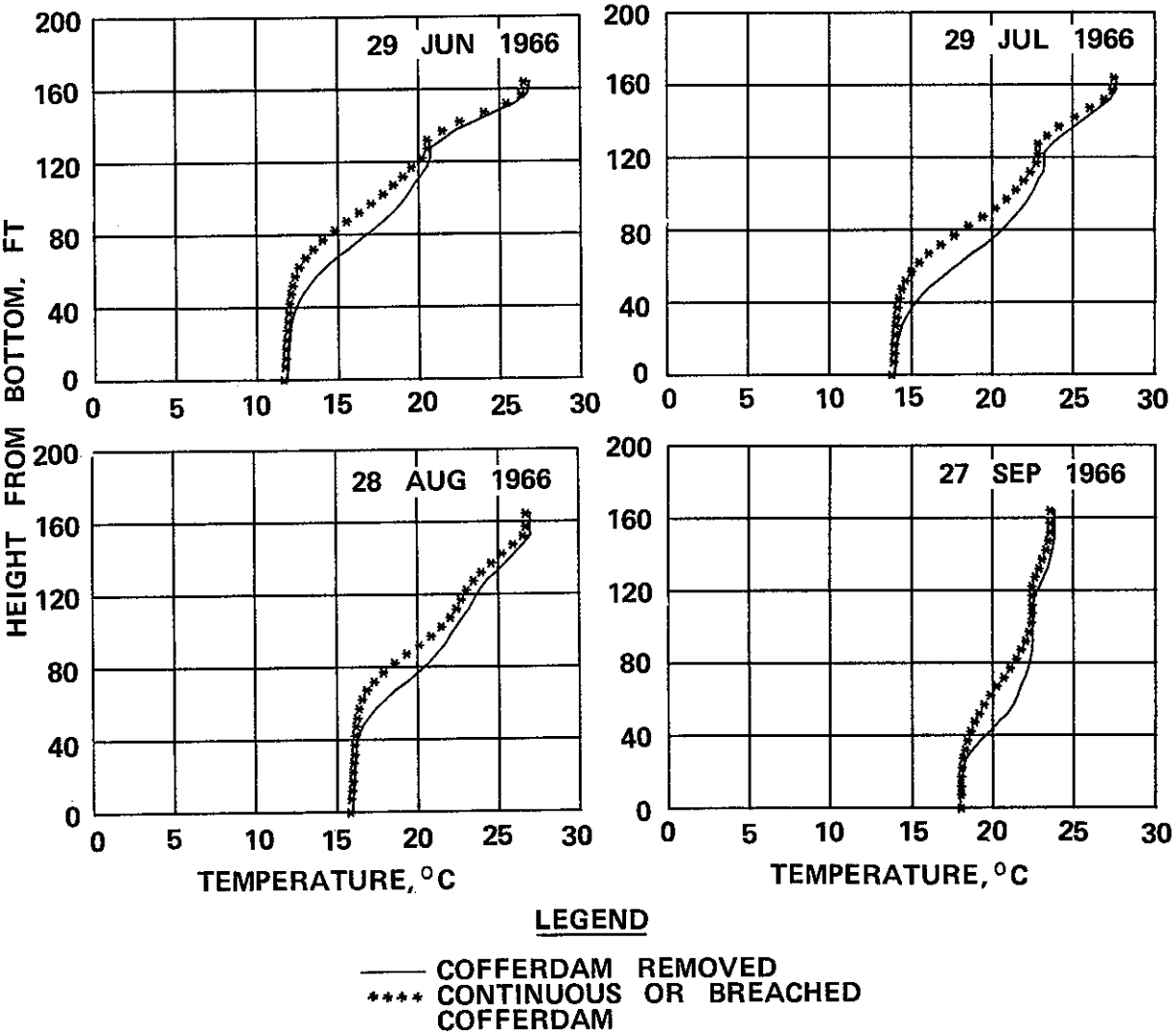

Figure 6. Predicted temperature distribution without the cofferdam and with the continuous or breached cofferdam

release D.O. concentration with the cofferdam either continuous or breached tended to be superior to those predicted with the cofferdam removed. These qualitative results are indicated in Figure 7. Essentially identical predictions were obtained for the breached (Option C) and continuous cofferdam (Option B) for the reasons indicated in paragraph 14. These qualitative results reflect the general trends but inherently do not quantify the relative merits of the respective geometrical configuration.

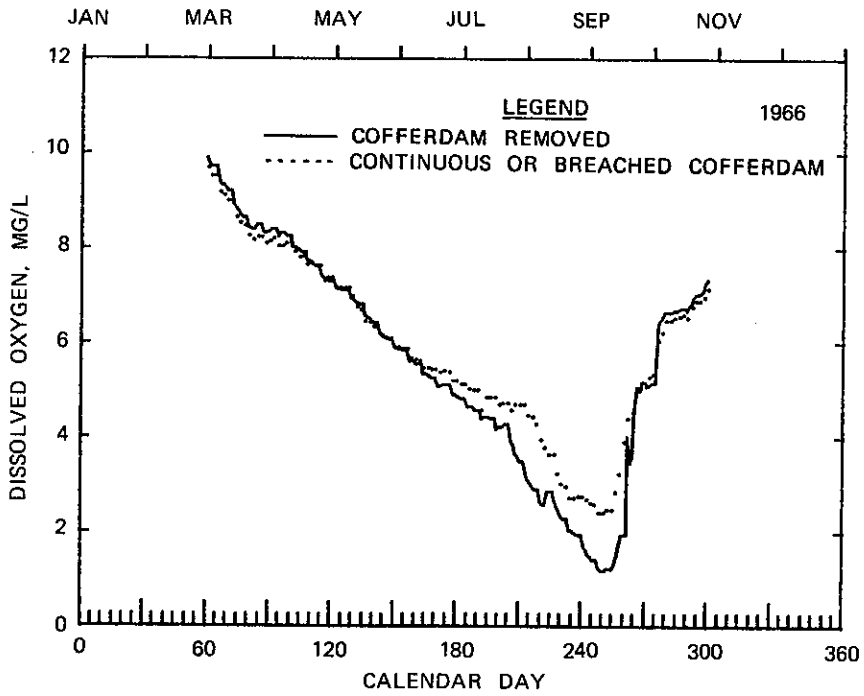

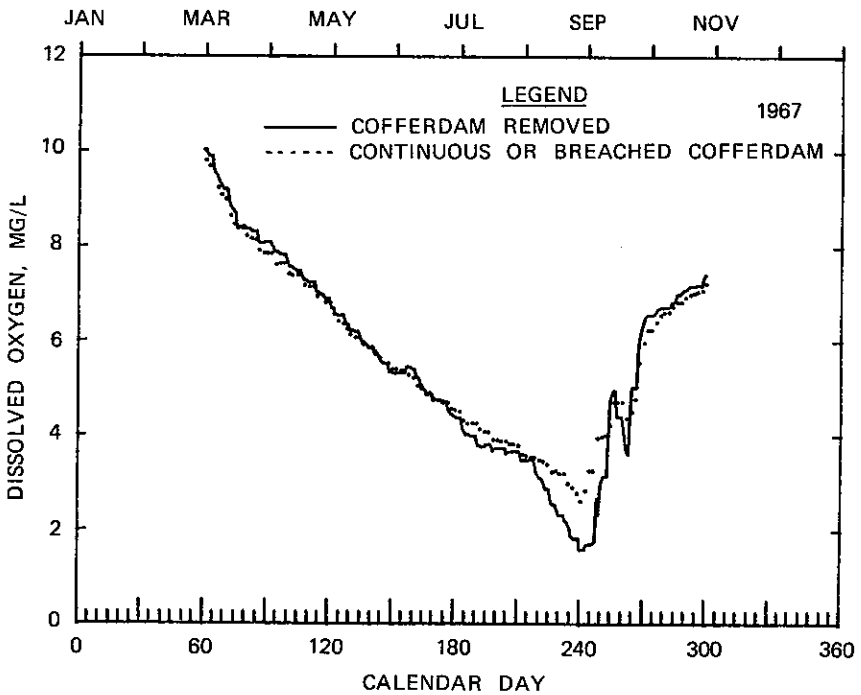

Figure 7. Predicted release D.O.

Quantitative results

21. Deviation plots for each simulation year are presented in Figure 8. The ordinate is the predicted release D.O. concentration with the cofferdam (Option B or C) minus the predicted D.O. with the cofferdam removed (Option A). A positive deviation indicates that the release D.O. concentration with the cofferdam would be greater by the indicated magnitude than that concentration release without the cofferdam.

22. Between 1 June and mid-July, the cofferdam resulted in slight improvement in the release D.O. as compared with that with the cofferdam removed. The magnitude of enhancement was somewhat erratic as a result of the dependency upon the hydrological and meteorological conditions; however, in all cases maximum improvement was less than 1 mg/ℓ and the average improvement over this time frame was no more than 0.7 mg/ℓ. Beginning in late July to mid-August, a period existed for each study year in which the D.O. enhancement was in excess of 1 mg/ℓ. This period varied from 25 to 58 days (depending on the study year) and the magnitude of D.O. enhancement generally varied between 1 mg/ℓ and 1.8 mg/ℓ. Only during 1966 did D.O. enhancement exceed 2 mg/ℓ and this was for only a three-day period. As indicated in Figure 8, the period of maximum D.O. enhancement dominates the deviation plot and the magnitude of D.O. enhancement usually drops rapidly on both sides of this region.

Idealized predictions of required injected oxygen

23. To withdraw water from the reservoir that has an average D.O. concentration of 6 mg/ℓ, oxygen would have to be added to the withdrawal zone in the reservoir during periods in which the volumetrically weighted average D.O. concentration in the release is less than 6 mg/ℓ. Typically, the release D.O. concentration was less than 6 mg/ℓ between mid-May and October (Figure 7). The idealized daily average injection rate required to eradicate deficits below 6 mg/ℓ was computed by multiplying the average daily release by the volumetrically weighted average D.O. below 6 mg/ℓ. Predicted daily average injection rates for 1966 are presented in Figure 9. Although the predicted injection histories are

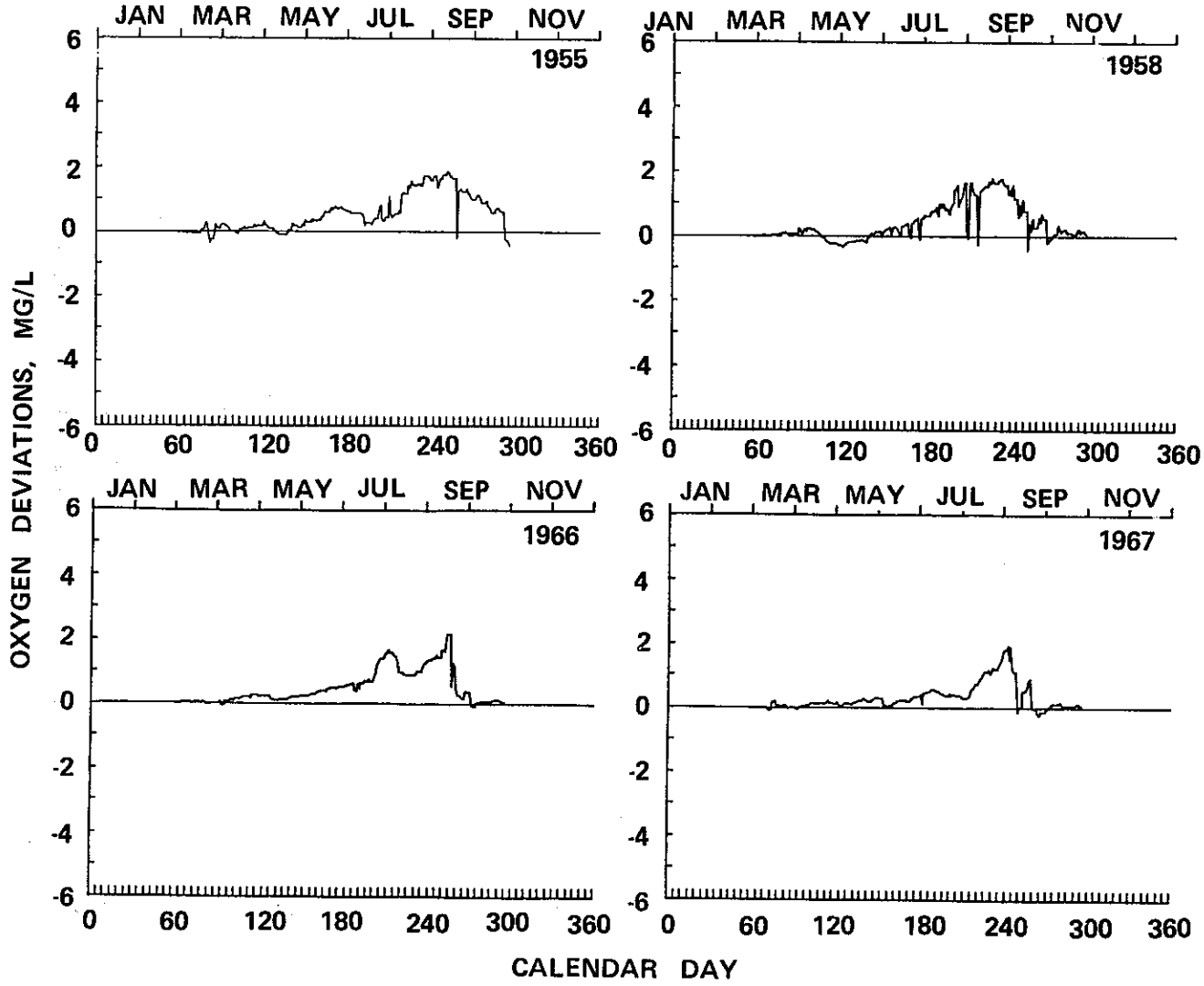

Figure 8. Predicted release D.O. with the cofferdam minus the predicted release D.O. with the cofferdam removed

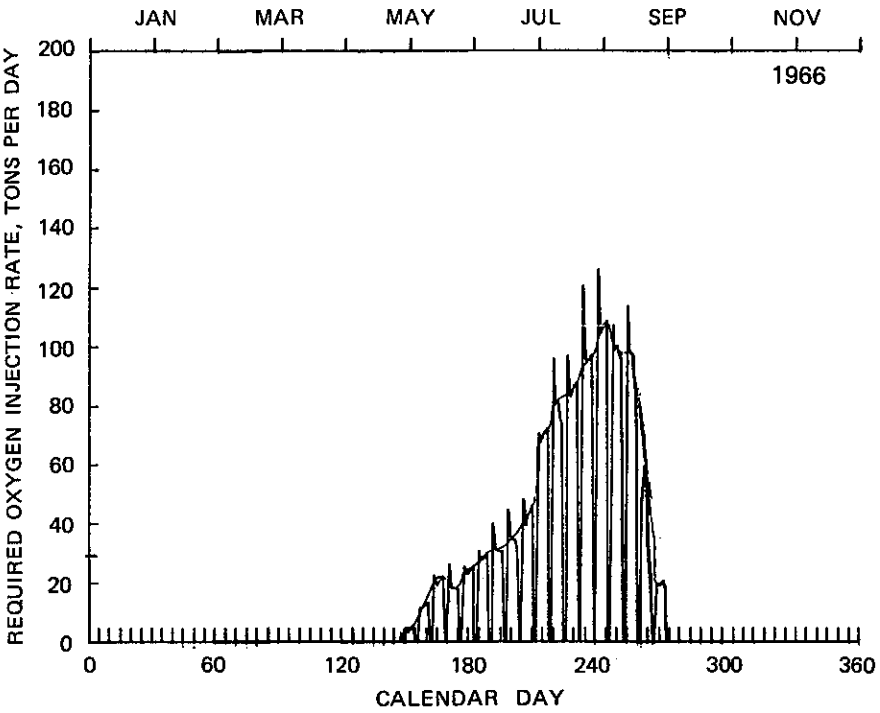

a. Cofferdam removed

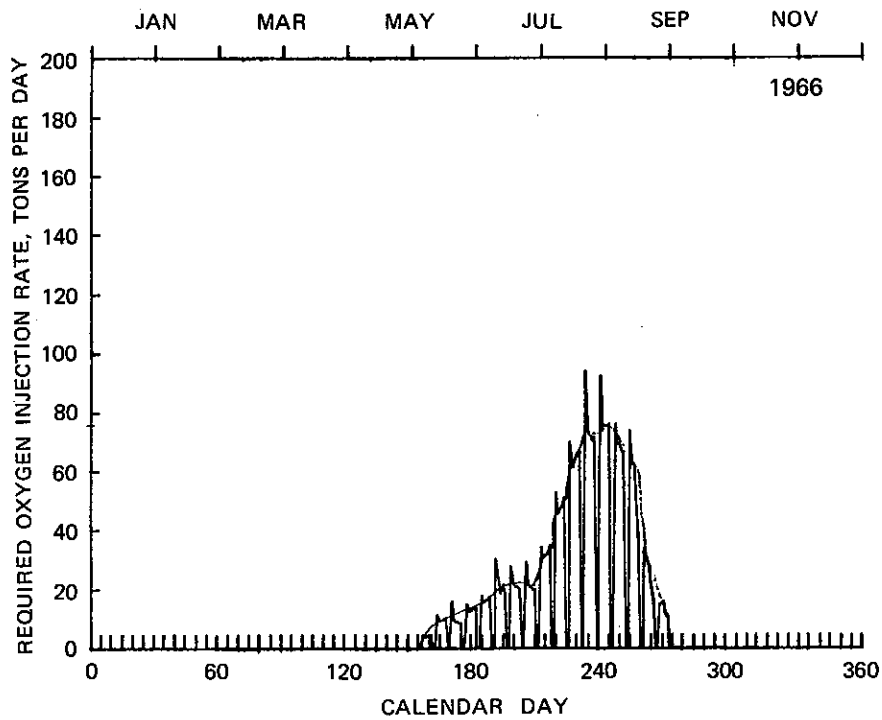

b. Continuous or breached cofferdam

Figure 9. Daily deficit in release D.O.

unique for each study year, these results are representative of the results for all simulation years.

24. The temporal injection rate required over a simulation depends upon a large number of variables. However, at any particular time it is essentially dependent upon (a) the vertical temperature and D.O. distributions and (b) the operational methodology. Both of these effects are apparent in Figure 9. During maximum stratification, the least favorable D.O. distribution develops in the metalimnion and hypolimnion. The center line of the penstock is approximately 70 ft below the surface and thus significant quantities of water are withdrawn from the metalimnion and hypolimnion. If large releases occur during periods of low D.O., large injection rates are required. Conversely, if small releases are made, smaller injection rates are required. Thus, the predicted injection rates reflect the coupling between operations and the D.O. in the withdrawal zone. Further, D.O. concentrations in the withdrawal zone varies rather slowly whereas the hydropower operations are highly transient. As a result, erratic daily injection rates are computed.

25. The maximum daily injection rate (neglecting spikes created by the operational strategy) computed for each study year is presented in the following tabulation:

	Computed Maximum Injection Rate tons per day		
Year	Cofferdam Removed	Continuous Cofferdam	Breached Cofferdam
1955	110	62	62
1958	97	55	55
1966	110	75	75
1967	95	70	70

26. A more comprehensive comparison of the respective injection rates can be made from the deviation plots for each simulation year (Figure 10). The ordinate is the predicted injection rate with the cofferdam minus the predicted rate with the cofferdam removed. A negative magnitude indicates that the required injection rate with the cofferdam

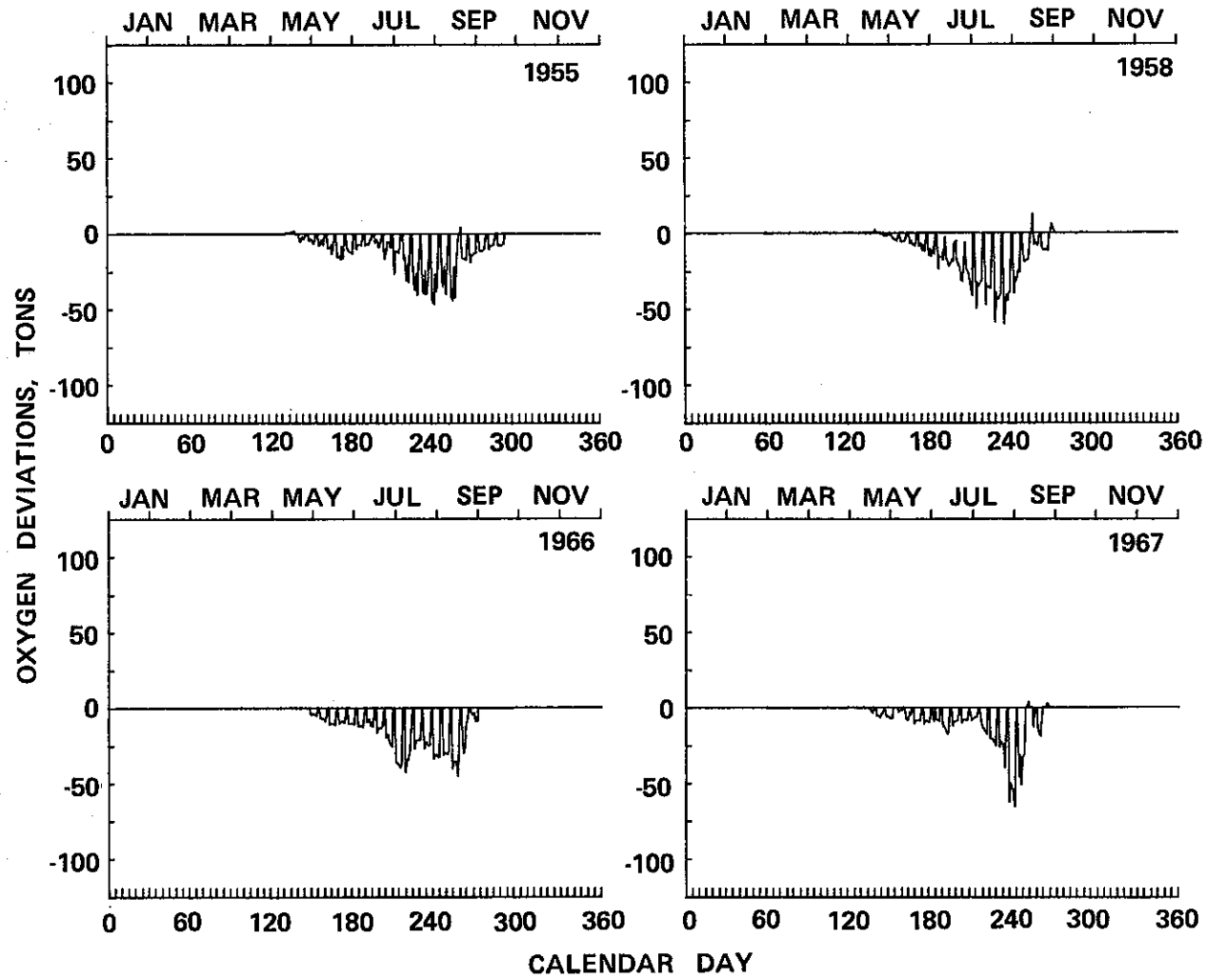

Figure 10. Computed differences in idealized injections rates. Rates with cofferdam (continuous or breached) minus rate without cofferdam

is the indicated magnitude less than that (predicted) without the cofferdam. As compared with removal, retention of the cofferdam consistently resulted in smaller required oxygen injection rates. In general, prior to mid-July and after September the difference in the predicted injection rate was relatively insignificant. During August and September the maximum difference in the predicted injection rates was between 35 and 50 tons per day (depending upon the simulation year).

27. The total quantity of oxygen required in the prototype for either (or both) in-reservoir geometries may be significantly different from those predicted by the above idealized computations. The required injected quantity will depend upon the efficiency of the particular injection system in enhancing the D.O. distribution within the unique withdrawal zone for the in-reservoir geometry selected. It is improbable that a particular injection system and operational scheme will be equally effective for all in-reservoir geometries investigated since the withdrawal and pumpback velocity distributions in the reservoir are different for various geometries. Thus, from idealized computations it is not possible to accurately deduce either quantitatively (or relatively) the injected oxygen required in the respective prototype configurations. These calculations serve as indicators based upon the integrated deficit and an idealized injection system.

Release Temperature

28. A representative temperature deviation plot is presented in Figure 11. A positive deviation indicates that the release temperature with the cofferdam would be larger by the indicated magnitude than that release without the cofferdam. The cofferdam resulted in slightly warmer releases because of the higher withdrawal distribution. The temperature increase during the stratification season was typically between 0.5 and 2°C. The duration of the increases was approximately six to eight months (depending upon the simulation year).

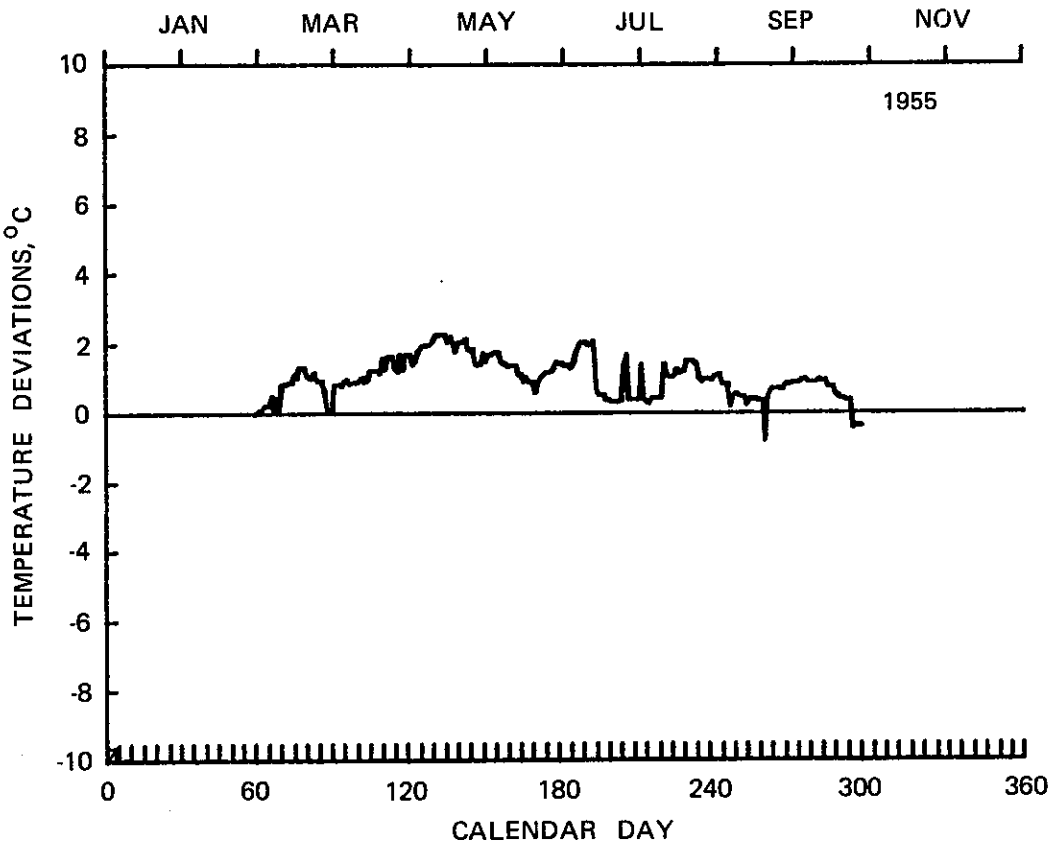

Figure 11. Predicted increase in release temperature if cofferdam is left in place as compared with removal

PART IV: CONCLUSIONS

29. The relative effectiveness and/or feasibility of four in-reservoir structural alternatives in enhancing reservoir and release water quality was predicted. Predicated upon analysis of these predictions, the alternatives should be ranked in the following order:

Rank	Option
1	Removal of the cofferdam
2	Continuous cofferdam
3	Breached cofferdam
4	Raised cofferdam

30. The least favorable option is the raised cofferdam. Even though release D.O. concentrations are increased by raising the crest to el 400, substantially reduced water quality may result in the reservoir. Reasonable depletion rates would result in a rather large anaerobic region in the hypolimnion. This occurs because the high crest elevation minimizes advection and vertical mixing at the deeper elevations. This option is not recommended.

31. Although the predicted water quality (both in the reservoir and in the release) was basically the same for the continuous and breached cofferdam, the latter option is not considered desirable. The breach provides a flow path below the crest of the cofferdam. Between pumpback and generation, gravity flow through the breach could result in lower quality water between the cofferdam and dam. During the subsequent hydropower release, a pulse of water with relatively low D.O. concentrations could be released. This flow process was observed in the physical model but significant investigation of this flow was outside the scope of the numerical study.

32. The effect of the cofferdam (continuous or breached) on the performance of the proposed RBRR oxygen injection system is unknown because the injection system was developed from pilot studies at Clarks Hill Reservoir which did not have a submerged cofferdam. Results from the physical model indicated that the cofferdam significantly

affects the hydrodynamics of both selective withdrawal and pumpback. As a result, the presence of a cofferdam could have an adverse effect upon the projected efficiency of the injection system in enhancment of the D.O. concentration in the withdrawal zone.

33. Any horizontal obstruction in the reservoir which reduces the water withdrawn from the hypolimnion by withdrawal or pumpback (entrainment) has the effect of decreasing vertical mixing and advection. The decreased mixing and increased residence time can result in a degradation in the D.O. distribution (with time) in the lower layers if oxygen demands exists. The impact of a depletion rate of 0.1 mg/ℓ/day upon the D.O. distribution during September of each study year is demonstrated in Figure 4. If severe loading exists in the hypolimnion, the impact could be more severe.

34. Removal of the cofferdam should complement the oxygen system. The proposed oxygen injection system is designed to enhance the D.O. distribution in the zone of withdrawal such that the flow-weighted average D.O. concentration is equal to or in excess of 6 mg/ℓ. At any particular time, the desired increase in the D.O. distribution depends upon the deficit and velocity distribution within the withdrawal zone. It is difficult to design an optimum variable rate system that matches this objective at all times because the deficit distribution varies with time. Thus, the system has to be designed for the maximum anticipated deficit. However, it must also be capable of distributing the oxygen appropriately within the zone of withdrawal. The characteristics of the withdrawal zone (location of the limits and velocity distribution) vary with the hydrological and meteorological conditions and the cofferdam configuration. Removal of the cofferdam should make designing an injection system less difficult. The enhanced vertical mixing that results from the pumpback process will tend to distribute the D.O. and make placement of oxygen within the withdrawal zone less critical.

35. The deeper withdrawal distribution that would result with the cofferdam removed would provide slightly cooler releases (1°C to 2°C) than with the other in-reservoir structural alternatives. During periods of relatively strong stratification, the release temperatures would be

more favorable. If the temperature criterion is exceeded, this geometrical alternative would tend to reduce its duration and intensity. This should be beneficial in meeting the coldwater temperature objective.

36. The sizing of the oxygen injection plant was outside the scope of the WES effort. Detailed development of the oxygen injection system by SAS is described in Design Memorandum 3. Idealized injection rates were included herein only to serve as indicators.

Table 1

A Synopsis of In-Reservoir D.O. Analysis

Geometry	Abbreviated Findings
(Option A) cofferdam removed	a. Tended to produce better D.O. distribution during early phases of stratification. b. Resulted in most favorable D.O. distribution in late periods of stratification as compared with other geometries.
(Option B) cofferdam left	a. D.O. distribution tended to be inferior to that of Option A during early period of stratification. b. Less favorable D.O. distribution in the hypolimnion during the late phases of stratification (as compared with Option A).
(Option C) breached cofferdam	a. Predicted D.O. distribution identical to unbreached case. b. Higher potential for pulses of lower D.O. releases than would occur with unbreached cofferdam (Option B).
(Option D) raised cofferdam	a. Produced anaerobic conditions in the hypolimnion between June and mid-July. Subsequently, the thickness of the anaerobic zone increased to between 65 and 80 ft by the end of September.

APPENDIX A: DISCUSSION OF NUMERICAL MODEL

Simulation Model Description

1. The downstream release characteristics and internal structure of temperature within a reservoir were predicted with a numerical simulation model. The model, hereinafter identified as WESTEX* was developed at the U. S. Army Engineer Waterways Experiment Station (WES) based on results of Clay and Fruh (1970), Edinger and Geyer (1965), Dake and Harleman (1966), Bohan and Grace (1973), Imberger,** and others.

Introduction

2. The reservoir is conceptualized as a number of homogeneous horizontal layers stacked vertically, and the heat sources and sinks to a general layer are represented as shown in Figure A1. The solution for the temperature history of a general layer (or control volume) is obtained by solving a conservation of mass and energy equation. The governing equation is:

$$\frac{\partial \theta}{\partial t} = \frac{Q_i \theta_i}{A\Delta Z} - \frac{Q_o \theta_o}{A\Delta Z} + \frac{1}{A}\frac{\partial}{\partial Z}\left(kA\frac{\partial \theta}{\partial Z}\right) - \frac{1}{A}\frac{\partial (Q_v \theta)}{\partial Z} + \frac{1}{\rho C_p A}\frac{\partial H}{\partial Z} \qquad \text{(A1)}$$

where

θ = temperature of layer, °F

t = time, days

θ_i = inflow temperature, °F

Q_i = flow rate into layer, ft^3/day

A = horizontal cross-sectional area, ft^2

ΔZ = layer thickness, ft

θ_o = outflow temperature, °F

Q_o = outflow rate, ft^3/day

Z = elevation, ft

---

* Bruce Loctice, "WESTEX--A reservoir Heat Budget Model" (first draft, unpublished), U. S. Army Engineer Waterways Experiment Station, CE, Vicksburg, Miss.

** Private communication, Imberger, and Jorg.

CONTROL VOLUME REPRESENTATION

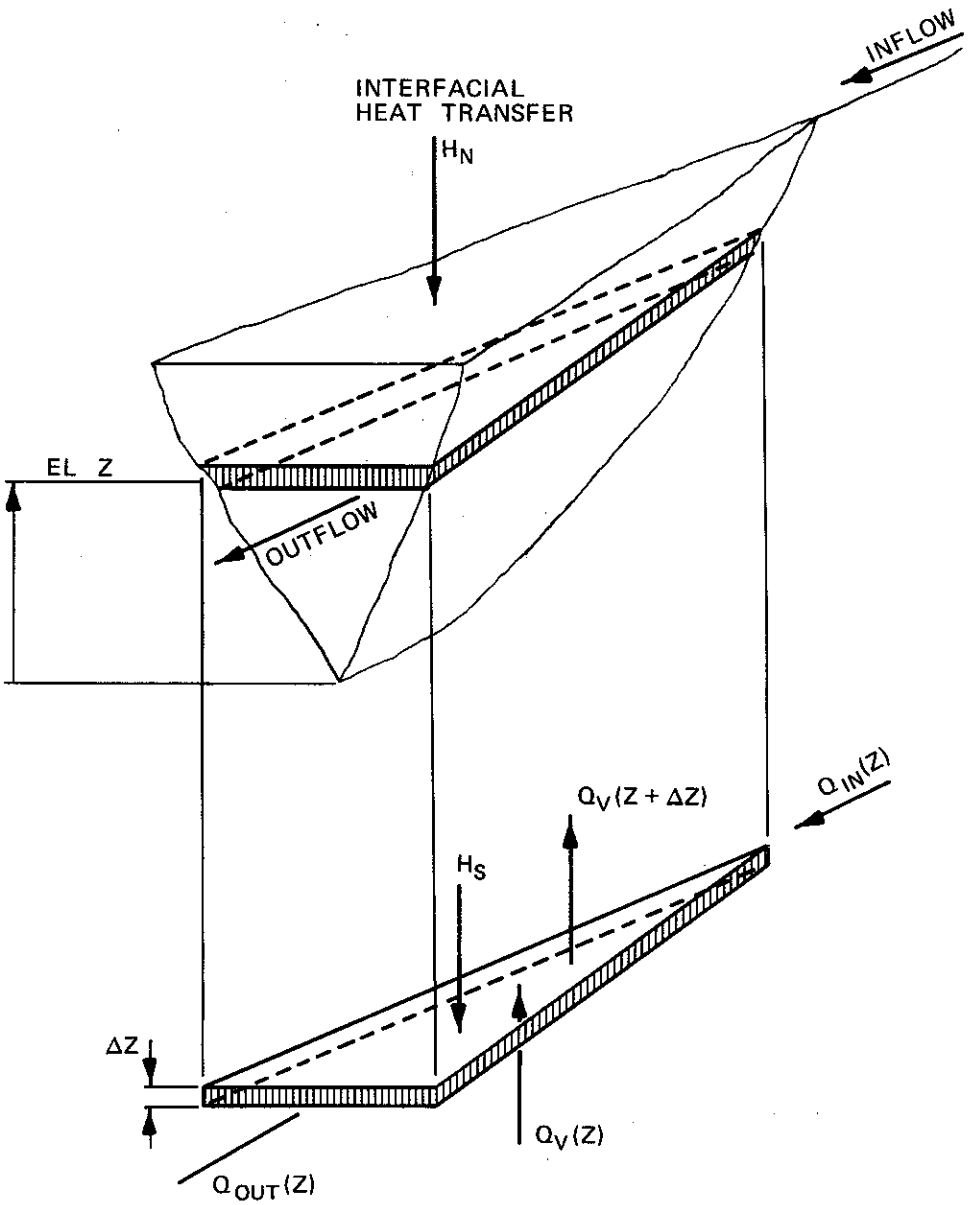

Figure A1. Typical layer in one-dimensional description

k = vertical diffusion coefficient, ft^2/day

Q_v = net vertical flow into or out of layer, ft^3/day

ρ = density of water, lb/ft^3

C_p = specific heat of water, Btu/lb/°F

$\partial H/\partial Z$ = external heat source, Btu/ft/day

Appropriate boundary conditions must be supplied at the air-water and the mud-water interfaces. Solution of Equation 1 for each layer through time yields the dynamic vertical temperature distribution of the reservoir.

3. Conservative water quality constituents are those parameters for which the concentration in an elemental volume is affected only by dilution, not by biological processes, chemical reactions, or physical phenomena such as gravity. Clay and Fruh (1970) demonstrated that suitable conservative constituents for simulation might include chloride, sulfate, sodium, or silica concentrations. Conservative constituent concentrations can be budgeted in a manner analogous to that used for the heat budget. Using conservation of mass, the change with respect to time of conservative constituent concentrations can be represented by:

$$\frac{\partial C}{\partial t} = \frac{Q_i C_i}{A\Delta Z} - \frac{Q_o C_o}{A\Delta Z} - \frac{1}{A}\frac{\partial (Q_v C)}{\partial Z} + \frac{1}{A}\frac{\partial}{\partial Z}\left(kA\frac{\partial C}{\partial Z}\right) \qquad \text{(A2)}$$

where

C = concentration of a conservative constituent, mg/ℓ

t = time, days

C_i = inflow concentration, mg/ℓ

Q_i = inflow rate, ft^3/day

A = cross-sectional area, ft^2

ΔZ = layer thickness, ft

C_o = outflow concentration, mg/ℓ

Q_o = outflow rate, ft^3/day

Q_v = net vertical flow, ft^3/day

Z = elevation, ft

k = vertical diffusion coefficient, ft^2/day

4. Bella (1970), Fruh and Davis (1972), and Markofsky and Harleman (1971) have demonstrated the application of a one-dimensional model to describe a nonconservative constituent budget. Nonconservative parameters can be budgeted similar to conservative parameters if the nonconservative processes are appropriately modeled. Bella's (1970) development of a one-dimensional model for dissolved oxygen (D.O.) structure of a reservoir yielded a governing equation similar to Equation 2 with an additional term representing the result of photosynthetic and respiration processes (source and sink terms). Fruh and Davis (1972) used one-dimensional models to describe vertical D.O. structures in a reservoir. The initial simulation of nonconservative processes with WESTEX was performed by Fontane and Bohan (1974) to analyze D.O. in Hartwell and Clarks Hill Reservoirs. Analysis of the D.O. distribution was accomplished in this study in a manner generally consistent with the work of Fontane and Bohan (1974). The upper, well-mixed layers in the reservoir were assumed to be approximately saturated (80 percent) with D.O. This degree of saturation was assumed to extend to the depth at which a temperature difference of 1°C from the surface temperature existed. A diffusion analogy similar to that for thermal diffusion (described in paragraph 15) was used to obtain the desired downward transport of D.O. below this depth. A constant daily D.O. depletion rate of 0.1 mg/ℓ was then applied to each layer below this depth in the reservoir. The selection of the 1.0°C temperature difference depth and the 0.1 mg/ℓ daily depletion rate was based on an analysis of observed temperature and D.O. profiles in Hartwell and Clarks Hill Reservoirs by Fontane and Bohan (1974).

5. Fundamental assumptions and the various processes addressed in the mathematical model will be discussed in the following sections.

Fundamental Assumptions

6. Reservoir hydrodynamic phenomena and a thermal energy balance are used to predict temperature profiles and release temperatures in the time domain. The model includes computational methods for simulating heat transfer at the air-water interface, advective heat due to inflow,

outflow, and pumpback processes, and the internal dispersion of thermal energy. The model is conceptually one-dimensional based on the division of the impoundment into discrete horizontal layers of uniform thickness. Assumptions include the following:

a. Isotherms are parallel to the water surface both laterally and longitudinally.

b. The water in each discrete layer is physically homogeneous.

c. Internal advection and heat transfer occur only in the vertical direction.

d. External advection (inflow, outflow, and pumpback) occurs as a uniform distribution within each layer.

e. Internal dispersion (between layers) of thermal energy is accomplished by a diffusion mechanism that combines the effects of molecular diffusion, turbulent diffusion, and thermal convection.

7. The surface heat exchange, internal mixing, and advection processes are simulated separately and their effects are introduced sequentially at time intervals. A simplified flow chart of the mathematical simulation procedure is presented in Figure A2. Each process will be discussed.

Surface Heat Exchange

8. The net heat exchange at the surface is composed of seven heat exchange processes:

a. Shortwave solar radiation.

b. Reflected shortwave radiation.

c. Long-wave atmospheric radiation.

d. Reflected long-wave radiation.

e. Heat transfer due to conduction.

f. Back radiation from the water surface.

g. Heat loss due to evaporation.

9. The surface heat transfer process is solved in the WESTEX model with an approach developed by Edinger and Geyer (1965). The thermal equation quantifying the net surface heat exchange (after some

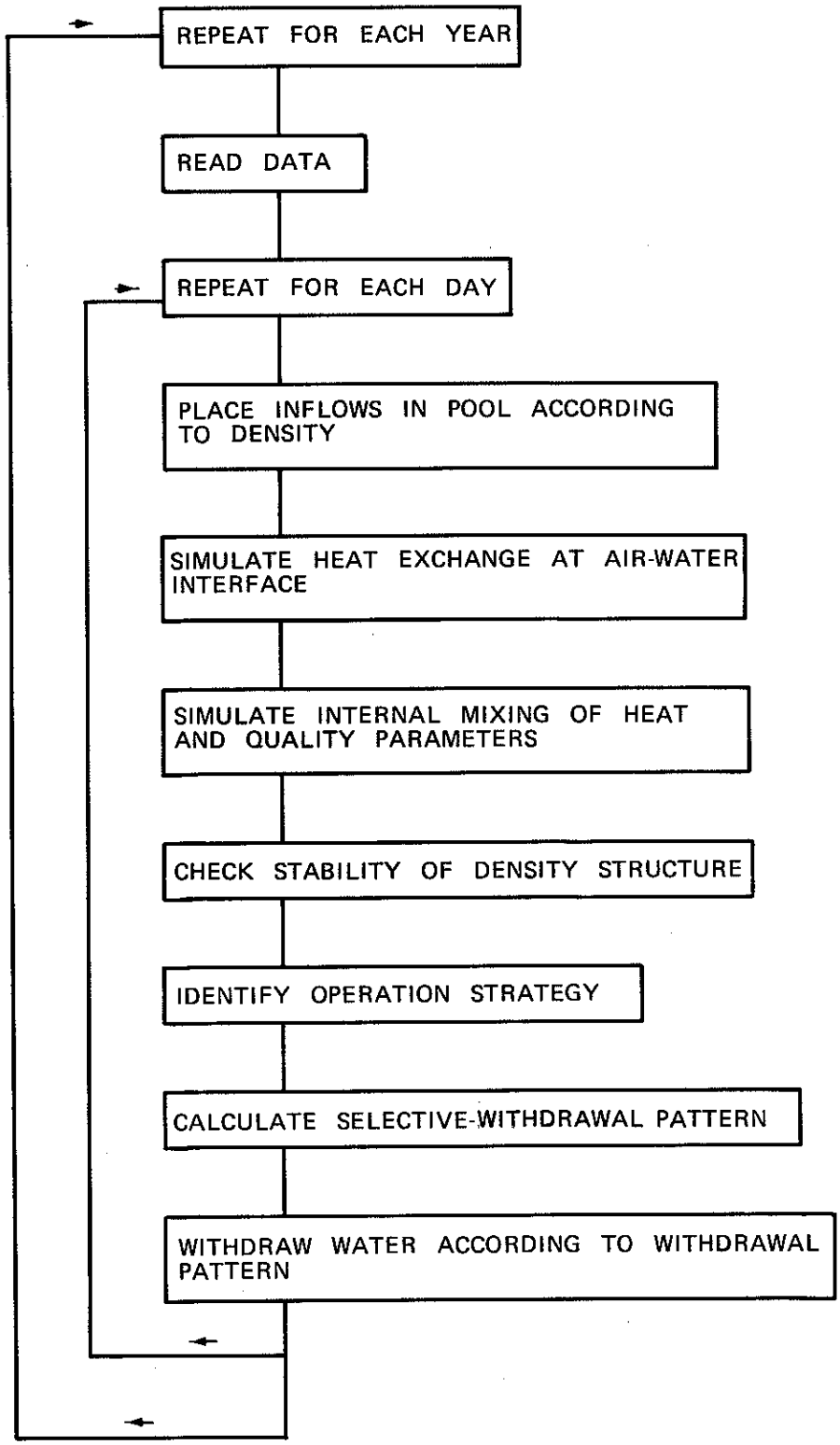

Figure A2. Simplified WESTEX flow chart

linearization) is:

$$H = K\ (E - \theta_S) \tag{A3}$$

where

H = net rate of surface heat transfer, Btu/ft^2/day

K = coefficient of surface heat exchange, Btu/ft^2/day/°F

E = equilibrium temperature, °F

θ_S = surface temperature, °F

Equilibrium temperature is defined as that temperature at which the net rate of heat exchange between the water surface and the atmosphere is zero. The coefficient of surface heat exchange is the rate of heat transfer at the air-water interface. The computation of equilibrium temperature and heat exchange coefficient is based solely on meteorological data as outlined by Edinger, Duttweiler, and Geyer (1968).

10. Heat from radiation, with the exception of shortwave radiation, is immediately absorbed at the surface or the top few feet. Depending upon the color and clarity of the water, shortwave radiation penetrates to and increases the temperature at greater depths. Based on laboratory investigations, Dake and Harleman (1966) have proposed an exponential decay with depth for describing the heat flux due to shortwave penetration. This approach is used in WESTEX.

11. The surface heat exchanges are implemented in the model by the placement of a percentage of the incoming shortwave radiation throughout the depth of the lake and by the placement of all other sources of surface heat exchange into the surface layer. The shortwave radiation is distributed exponentially, so that most is absorbed in the top layers and relatively little is absorbed in the lower layers. The procedure can be expressed mathematically by the following two equations:

$$H_s = K(E - \theta) - (1 - \beta)\chi \tag{A4}$$

$$H_i = (1 - \beta)\ \chi e^{-\lambda z_i} \tag{A5}$$

where

H_s = heat transfer rate into or out of the surface layer, $Btu/ft^2/day$

β = percentage of the shortwave radiation absorbed in the surface layer

χ = total incoming shortwave radiation rate, $Btu/ft^2/day$

H_i = rate of heat absorption in layer i, $Btu/ft^2/day$

e = natural logarithmic base (2.7183)

λ = heat absorption coefficient, ft^{-1}

z_i = depth below surface, ft

12. Equations A4 and A5 are applied to the temperature profile once during each one-day time-step. The net heat exchange rate into each layer is computed and converted into a temperature change. The temperature changes are used to determine an updated temperature profile for the lake.

Inflow

13. The inflow process is simulated in three basic steps. The point of neutral buoyancy of the inflow current is found, water in the lake is displaced and mixed upward, and the water in the lake is mixed with the inflow.

14. The point of neutral buoyancy is found by a linear interpolation or extrapolation upon the density profile of the lake. The inflow volume is allocated to the layer of neutral buoyancy. Where inflow volume into a layer (i) exceeds the physical capacity of the layer (i), the excess volume is added to the volume of the next higher layer (i + 1). The excess volume from layer i (which is added to layer (i + 1)) is mixed with the volume in layer (i + 1). If the volume in layer (i + 1) after mixing is greater than the physical capacity of layer (i + 1), the excess mixed volume is placed in the next layer (i + 2). The sequential mixing process is repeated until the inflow is distributed within the water column.

Internal Mixing

15. The internal dispersion process is represented by a mixing scheme mathematically similar to a simple diffusion analogy. The mixing process is used to account for the effects of molecular diffusion, turbulence diffusion, and additional internal mixing processes which are not explicitly addressed. Internal mixing transfers heat and other water quality constituents (e.g., D.O.) between adjacent layers. The magnitude of the transfer between two layers in the WESTEX model is expressed as a percentage of the total transfer required to mix the two layers. This percentage is a mixing coefficient that is defined for every layer. Data input includes values of the mixing coefficient at the maximum pool elevation (α_1) and at the bottom of the lake (α_2). The values are predicated upon field data if available. The exponential fit between the two extreme values is used to determine the appropriate coefficient for each layer. The same coefficients are used for mixing qualities as for mixing heat.

Outflow

16. The outflow component of the model incorporates the selective withdrawal techniques for orifice flow developed at WES (Bohan and Grace 1973). Additionally, the selective withdrawal description was analyzed to include the appropriate application to simultaneous releases from multiple horizontal ports. Transcendental equations define the location of zero-velocity limits and are solved with a half-interval search method. The location of the zero-velocity limits is functionally dependent on the geometric configuration of the withdrawal device, release flow rates, and density structure within the lake. With knowledge of the limits of the withdrawal zone, the velocity profile produced by the outflow can be determined. The flow from each layer is then computed as the product of the velocity in the layer and the width and thickness of the layer. A flow-weighted average is applied to the temperature and D.O. profiles to determine the value of the release temperature and

D.O. concentration for each flow condition.

Operation Schedules

17. Because the generation and pumpback flow rates vary considerably during a day's operation and these flow rates affect withdrawal and pumpback characteristics, it was not adequate to use daily average flows to accurately simulate generation and pumpback operations. Daily average flow routings usually are quite accurate for less dynamic reservoirs such as water supply and flood-control projects. For this model, the planned generation and pumpback flow rates and durations (in hours) are used rather than daily averaged flow rates. The model can handle a variety of different flow conditions within a simulation day. Input includes modes of operation (generation or pumpback), flow rates, and durations of flow for each day.

Pumpback Characteristics

18. For numerical simulations it is necessary to define the temperature and D.O. content of the flow pumped from the tailrace of Clarks Hill Lake into RBRR. The pumpback operation was modeled by mixing the release volume from RBRR with an equivalent surface volume from Clarks Hill. It should be noted that pumpback flows containing 25 and 75 percent (by volume) of Clarks Hill water were also simulated. In this range, the fraction of pumpback (assumed to be contributed from Clarks Hill) had little impact on the release water quality. The temperature and D.O. of the contribution from RBRR is known from previous generation cycles. The surface temperature for Clarks Hill is assumed to be the surface temperature of RBRR. The D.O. content of the contribution from Clarks Hill is saturation corresponding to the surface temperatures of RBRR.

19. The physical model (described in Appendix B) was used to determine the source, magnitude, and distribution of the reservoir waters entrained into the pumpback jet. Removal of the entrained volume from the reservoir is mathematically simulated in a manner analogous to

the outflow process, except that the outflow quantity and quality are mixed with the pumpback volume. Placement and mixing in the reservoir of the augmented pumpback volume are analogous to the inflow process described in paragraph 13.

Density Stability

20. The WESTEX model requires a stable density profile prior to outflow. Stability is assured by searching adjacent layers from bottom to top comparing densities. If a density instability is identified, the two unstable layers are partially mixed, and the mixed density is compared with the density of the layer above the mixed region. If an instability still remains, the layer above the mixed region is included in the mixed region; and the process continues until stability is achieved or the surface is reached. By mixing layers above an instability it is possible to create an instability below the mixed region. If such an instability is detected, then mixing proceeds downward until stability is achieved or the bottom is reached.

REFERENCES

Bella, D. A. 1970. "Dissolved Oxygen Variations in Stratified Lakes," Journal, Sanitary Engineering Division, American Society of Civil Engineers, Vol 96, No. SA5, Paper No. 7628, pp 1129-1146.

Bohan, J. P., and Grace, J. L., Jr. 1973 (Mar). "Selective Withdrawal from Man-Made Lakes; Hydraulic Laboratory Investigation," Technical Report H-73-4, U. S. Army Engineer Waterways Experiment Station, CE, Vicksburg, Miss.

Clay, H. M., Jr., and Fruh, E. G. 1970. "Selective Withdrawal at Lake Livingston; An Impoundment Water Quality Model Emphasizing Selective Withdrawal," Progress Report EHE 70-18 (CRWR 66), Environmental Health Engineering Research Laboratory, University of Texas, Austin, Tex.

Dake, J. M. K., and Harleman, D. R. F. 1966. "An Analytical and Experimental Investigation of Thermal Stratification in Lakes and Ponds," Technical Report No. 99, Massachusetts Institute of Technology Hydrodynamics Laboratory, Cambridge, Mass.

Edinger, J. E., Duttweiler, D. W., and Geyer, J. C. 1968. "The Response of Water Temperature to Meteorological Conditions," Water Resources Research, Vol 4, No. 5, pp 1137-1143.

Edinger, J. E. and Geyer, J. C. 1965. "Heat Exchange in the Environment," Publication No. 65-902, Edison Electric Institute, New York, N. Y.

Fontane, D. G., and Bohan, J. P. 1974 (Dec). "Richard B. Russell Lake Water Quality Investigation; Hydraulic Laboratory Investigation," Technical Report H-74-14, U. S. Army Engineer Waterways Experiment Station, CE, Vicksburg, Miss.

Fruh, E. G., et al. 1972. "Limnological Investigations of Texas Impoundments for Water Quality Management Purposes," Final Report EHE 72-6 (CRWR 87), University of Texas, Austin, Tex.

Markofsky, M., and Harleman, D. R. F. 1971. "A Predictive Model for Thermal Stratification and Water Quality in Reservoirs," Report No. 134, Department of Civil Engineering, Massachusetts Institute of Technology, Cambridge, Mass.

APPENDIX B: DISCUSSION OF NEAR-FIELD PHYSICAL MODEL INVESTIGATION

Purpose

1. An undistorted-scale three-dimensional near-field model of the RBRR project was constructed in order to evaluate the effect of various cofferdam configurations upon the withdrawal and pumpback characteristics of the project. This information was used in conjunction with a numerical simulation model to determine which design option was most beneficial in meeting release requirements for temperature and D.O. at the project.

Model Description

2. The physical model (Figure B1) was constructed to a 1:150 scale (model to prototype) and reproduced the area of the project between the dam and a point approximately 3000 ft upstream (shown in Figure B2). Prototype penstock intakes (Figure B3) were also modeled upstream of the transition from a circular to a rectangular cross section. Topography was reproduced with shaped urethane foam, plywood, sheet metal, and clear acrylic plastic. The cofferdam was constructed of sheet metal to simplify modifications to the model for each cofferdam configuration. Operation of each model penstock was controlled by a ball valve. These valves were either fully opened or closed during withdrawal and were adjusted to equally distribute flow through the four units operating during pumpback. Units 1 through 4 are reversible turbines; the remaining units 5 through 8 were constructed similarly but without the capability for pumpback operations.

Experimental Procedure

3. During selective withdrawal testing of all options, the outflow through each penstock was held constant at 7500 cfs. Pumpback flow was constant at 20,000 cfs and divided equally between the four

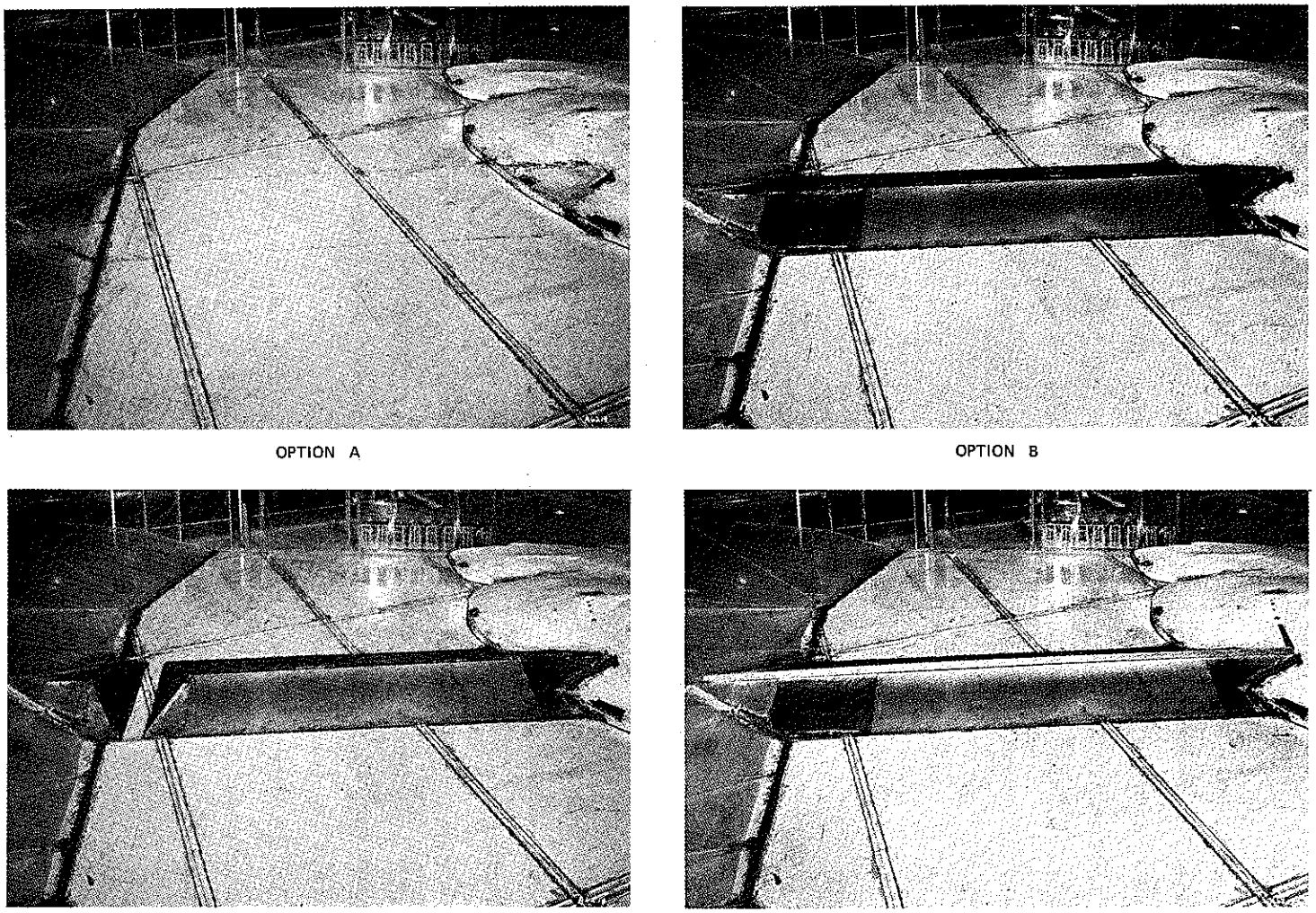

Figure B1. Physical model of RBRR, 1:150 scale

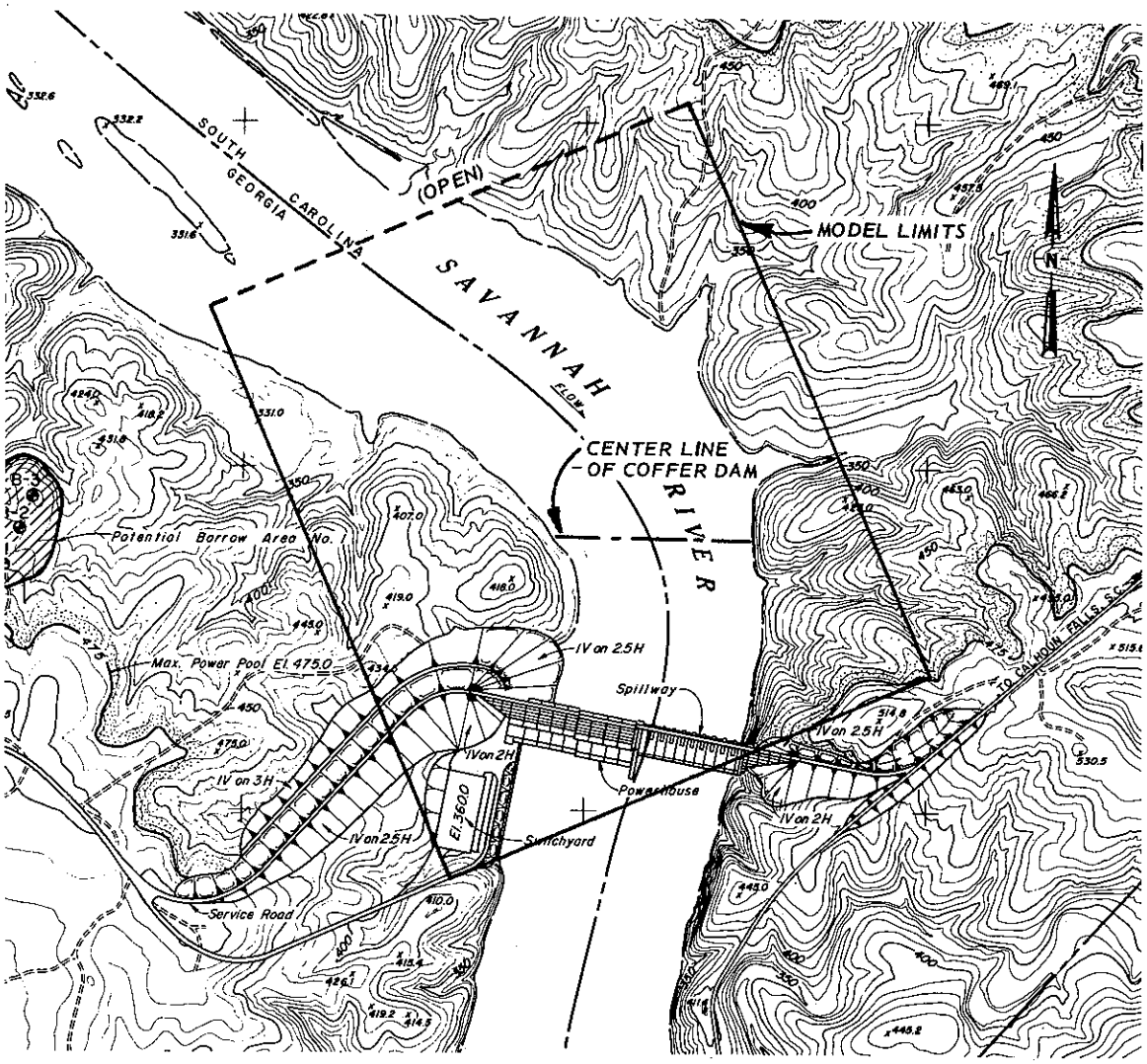

Figure B2. Limits of the RBRR physical model

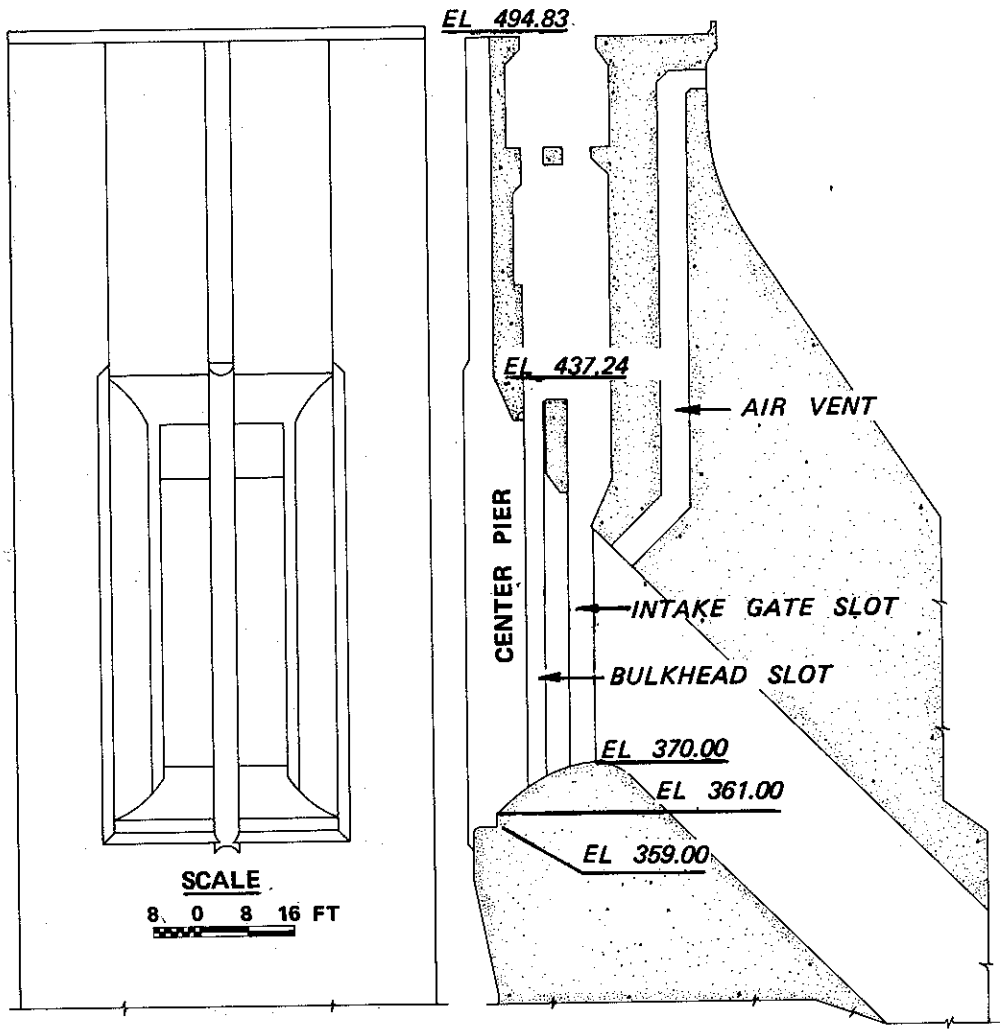

Figure B3. RBRR powerhouse intake

reversible units. Variations in total outflow rates were determined by the number of penstocks withdrawing from the reservoir. The majority of the tests were conducted with two, four, or six penstocks in operation.

4. Stratification was established in the model using fresh and saline waters to simulate the density distribution expected in the pool during the summer stratification period. An initial density profile was determined and outflow was initiated at the desired test flow. Vertical dye streaks were used to observe the formation of the withdrawal zone and to determine when steady-state conditions were established. After establishment of steady-state conditions, displacement of the vertical dye streaks was recorded on a video recorder and subsequently the velocity distribution and limits of withdrawal were determined.

5. Entrainment was determined for the pumpback tests by measuring the dilution of the pumpback jet with a fluorescent dye. The epilimnion or the hypolimnion was dyed in separate tests and the contribution of each to the total pumpback volume was measured. The total pumpback volume consisted of the volume of epilimnion and hypolimnion waters entrained plus the volume of the pumpback jet. Additionally, dye streaks were used to indicate the distribution of flow within the model during the pumpback operation.

Testing

6. Model tests were divided into four options with each option representing a different upstream cofferdam configuration. Option A simulated removal of the upstream cofferdam prior to filling the lake. Option B simulated the cofferdam as initially constructed with crest at el 378. In Option C, the Option B design was breached to simulate the planned second-stage diversion. In Option D, the same cofferdam described in Option B was modified with a sheet-pile wall to raise the crest to el 400.

Analysis

7. In the analysis of model data, the penstocks were treated as orifices and the cofferdam was treated as a submerged weir. In many cases, the analysis was conducted using the same dimensionless groupings employed by Bohan and Grace. They experimentally investigated the stratified flow field produced by withdrawal through orifices (circular and rectangular) and over submerged weirs. The weir study focused on flow over a weir in which the thermocline was below the crest of the weir. Bohan and Grace determined dimensionless groupings that characterized the flow regime and subsequently developed semiempirical descriptions of the withdrawal regime for the condition investigated. These descriptions were incorporated into the numerical routine SELECT. However, the flow conditions in RBRR included a number of geometrical and flow conditions for which SELECT was not developed. These included:

a. Multiple horizontal ports.

b. Bellmouthed intake geometrics.

c. Submerged weir with crest elevation below the elevation of the thermocline.

Thus, a near-field physical model was constructed to acquire the experimental data required to develop a description of the unique withdrawal characteristics applicable to RBRR. A review of the selective withdrawal descriptions developed for the various geometrical configurations will be discussed in four sections. They are:

a. Option A: cofferdam removed.

b. Option B: cofferdam left in place (with el 378).

c. Option C: cofferdam left in place with a second-stage diversion breach.

d. Option D: cofferdam crest raised from el 378 to el 400.

8. The subsequent discussion of the results obtained from Option A includes an overview of the idealized selective withdrawal work of Bohan and Grace. The Bohan and Grace descriptions were used for flow conditions in which the SELECT assumptions were valid. Discussion of the specific hydrodynamic effects, and the descriptions characterizing these

effects, introduced for RBRR will be given thereafter. Additionally, at the close of this appendix the hydrodynamic considerations of pumpback operation are discussed for each option.

Option A

9. In Option A, the cofferdam was removed leaving the approach upstream of the dam unobstructed. This was somewhat similar to a configuration studied by Bohan and Grace. They found that the upper and lower limits of the withdrawal zone should be described as a function of the densimetric Froude number such that

$$V_o = \frac{Z^2}{A_o}\left(\frac{\Delta\rho}{\rho}\, gZ\right)^{1/2} \tag{B1}$$

where

V_o = average velocity through the penstock, fps

Z = vertical difference in the elevation of the limit in question and the center line of the orifice, ft

A_o = area of the penstock, ft^2

$\Delta\rho$ = density difference of fluid between the elevations of the center line of the orifice and the limit in question, g/cc

ρ = density at the elevation of the center line of the orifice, g/cc

g = acceleration due to gravity, ft/sec^2

The quantity

$$\frac{V_o}{\sqrt{\frac{\Delta\rho}{\rho}\, gZ}}$$

is defined as the densimetric Froude number, where $g\Delta\rho/\rho$ represents the gravitational effect. Bohan and Grace found that this function was valid for both upper and lower limits of withdrawal, except in cases where the upper and lower limits intersected either the free surface or the bottom boundary, respectively.

10. Bohan and Grace predicted the location of maximum velocity from the following equation

$$\frac{Y_L}{H_L} = \left[\sin\left(\frac{1.57Z_L}{H_L}\right)\right]^2 \quad \text{(B2)}$$

where

Y_L = distance from lower limit to location of maximum velocity, ft

H_L = thickness of withdrawal zone; distance from lower limit to upper limit, ft

Z_L = distance from lower limit to orifice center line, ft

They found that the velocity profile above or below the elevation of maximum velocity could be calculated for boundary interference by:

$$\frac{V}{V_{max}} = 1 - \left(\frac{y\Delta\rho_v}{Y\Delta\rho_{max}}\right)^B \quad \text{(B3)}$$

and for the case when the withdrawal zone is not limited by a boundary:

$$\frac{V}{V_{max}} = \left(1 - \frac{y\Delta\rho_v}{Y\Delta\rho_{max}}\right)^N \quad \text{(B4)}$$

where

B = 2 for orifice and weir flow

N = 2 for orifice flow

N = 3 for weir flow

V/V_{max} = ratio of local velocity to maximum velocity

y = magnitude of distance from elevation of maximum velocity to some local elevation, ft

Y = magnitude of distance from elevation of maximum velocity to the withdrawal limit of interest, ft

$\Delta\rho_v$ = density difference between elevation of maximum velocity and local elevation, g/cc

$\Delta\rho_{max}$ = density difference between elevation of maximum velocity and the withdrawal limit of interest, g/cc

11. Analysis of data obtained in Option A tests indicated that

some of the descriptions in SELECT could be used to characterize selective withdrawal in RBRR. Equation B1 was used to predict the upper limits and Equation B2 was used to predict the point of maximum velocity. A new description for the lower limit of withdrawal was required. Analysis of the observed lower limits for Option A yielded the following description:

$$V_o = \left(\frac{Z_L^2}{A_o}\right)^{0.475} \left(\frac{\Delta\rho}{\rho} g Z_L\right)^{1/2} \tag{B5}$$

12. Equations B3 and B4 were applicable for Option A. Analysis of the data indicated that the appropriate values of the exponents B and N were 1.40 and 4.15, respectively.

Option B

13. Option B examined the hydrodynamic effects introduced by leaving the cofferdam in place. The cofferdam would be submerged with a nominal crest elevation of 378. The elevation of the thermocline will be above the weir crest. Previous studies have primarily addressed withdrawal characteristics of submerged weirs with crests above the elevation of the thermocline. As a result several new descriptions had to be developed.

14. The controlling flow structure, either the weir or the penstock, was found to be different for each of the two limits. The functional relationships for the upper limit were found to be influenced by penstock effects; those of the lower limits were affected by weir effects. Thus, no single functional form could be obtained that was adequate for the description of both limits. The equation which most adequately described the position of the upper limit of withdrawal for Option B was

$$V_o = 1.13 \left(\frac{H_o + Z_u}{Z_u}\right)^{1.05} \left(\frac{\Delta\rho}{\rho} g Z_u\right)^{1/2} \tag{B6}$$

where

H_o = vertical distance from bottom of lake to center line of orifice, ft

Z_u = vertical distance from the elevation of the orifice center line to the upper limit of withdrawal, ft

and all other parameters are defined in Equation B1.

15. The lower limit of withdrawal was modeled in a similar manner as the upper limit. The densimetric Froude number was slightly redefined for weir control as

$$F_w = \frac{V_w}{\left(\frac{\Delta\rho_w}{\rho_w} gZ_{WL}\right)^{1/2}}$$

where

F_w = redefined densimetric Froude number for weir flow

V_w = average velocity over the weir, fps

$\Delta\rho_w$ = density difference of fluid between the elevations of the weir and lower limit, g/cc

ρ_w = density of fluid at the elevation of the weir, g/cc

g = acceleration due to gravity, ft/sec^2

Z_{WL} = vertical distance from the elevation of the weir crest to the lower limit of the withdrawal, ft

Analysis of the Option B observed lower limits resulted in the following description

$$V_w = 21.0 \left(\frac{Z_{WL}^2}{Area}\right)^{1.15} \left(\frac{\Delta\rho_w}{\rho_w} gZ_{WL}\right)^{1/2} \qquad (B7)$$

where Area equals area of flow between the elevations of the upper limit of withdrawal and the weir crest, ft^2.

16. The point of maximum velocity for Option B was defined by

$$\frac{Y_L}{H_L} = 1.19\left(\frac{Z_{WL}}{H_L}\right) + 0.093 \qquad \text{(B8)}$$

17. Analysis of Option B test results indicated that Equations B3 and B4 were applicable with the appropriate values of exponents B and N which were determined to be 2 and 1.275, respectively. With these values, Equations B3 and B4 were used to describe the velocity profile.

Option C

18. In Option C, a diversion breach with the bottom at el 310 was placed on the east side of the cofferdam with a crest at el 378. Comparison of the outflow densities from Options B and C indicated that only 3 percent of the total outflow was withdrawn through the breach. Consequently, the descriptive equations developed for Option B apply to Option C. The breach was numerically modeled as an orifice with a center line at el 350 and an 8500-sq-ft area. Except for the breach, the cofferdam was identical to that simulated in Option B.

Option D

19. In Option D, the crest of the cofferdam would be raised from el 378 to el 400 by installing sheet piling. Analysis of the observed velocity profiles indicated that the location of the upper limit was controlled by flow over the cofferdam as compared with control by the penstocks with the Option B cofferdam crest at el 378. Analysis of the density differences and distances between the crest and the upper limit as a function of the number of penstocks operating in the model resulted in the equation

$$\frac{\Delta\rho_{wu} Z_{wu}}{\rho_w H_w} = 0.033 N_p^2 \qquad \text{(B9)}$$

where

$\Delta\rho_{wu}$ = density difference of fluid between the elevations of the cofferdam crest and the upper limit, g/cc

Z_{wu} = vertical distance from the elevation of the cofferdam crest to the upper limit, ft

H_w = height of the cofferdam, ft

N_p = number of penstocks in operation

Equation B9 is site specific and was developed for an H_w equal to 89 ft.

20. The lower limit was controlled by the cofferdam in a manner similar to that seen in Option B tests. As a result, the lower limit was described by Equation B7.

21. The location of the point of maximum velocity was a function of the position of the lower limit. The relationship developed from the data was

$$\frac{Y_L}{H_w} = 0.949 \left(\frac{Z_{WL}}{H_w}\right) + 0.235 \qquad \text{(B10)}$$

This equation is project specific and may not be applicable to other projects.

22. The shape of the boundary unaffected velocity profile determined for Option D data is described by the equation

$$\frac{V}{V_{max}} = 1 - \left(\frac{y\Delta\rho_v}{Y\Delta\rho_{max}}\right)^{2.48} \qquad \text{(B11)}$$

23. The boundary controlled velocity profile description developed for Option B was also valid for Option D.

Pumpback Results

24. The proposed operations schedule indicates that pumpback will be initiated very soon after the end of the afternoon generation period. Therefore, withdrawal currents were set up in the model prior to simulating the pumpback operation. Pumpback flow entered the model through units 1 through 4 at 5000 cfs per unit. The density of the pumpback was equal to or less than that of the outflow, depending on surface water conditions in Clarks Hill Lake.

Option A

25. Due to the 45-deg inclination of the penstocks the pumpback flow was directed to the water surface and subsequently deflected downward in the lake approximately 150 ft in front of the penstocks. After plunging, the pumpback current rose to a level of neutral density and spread laterally as a density current between the epilimnion and hypolimnion of the reservoir. A schematic of the flow pattern is presented in Figure B4. Dilution measurements using rhodamine-wt fluorescent dye indicated that the final volume of the density current produced by near-field entrainment was 2.5 times the pumpback volume. Fluorescent dye measurements and dye streak displacement observations indicated that 96 percent of the entrained volume came from below the thermocline. Although the velocity did not vary with depth in the entrained current from the hypolimnion, the entrained volume varies with depth because cross-sectional area of flow varies with depth.

Option B

26. The pumpback flow was similar to that observed in Option A tests except that a small amount of the pumpback volume was laterally deflected by the cofferdam to each side. Most of the flow traveled upstream at an elevation just above the cofferdam crest. As the flow reached a point approximately 500 ft upstream of the cofferdam, the pumpback jet began to transform to a density current.

27. Most of the entrained flow was from the hypolimnion as in Option A with the entrained flow crossing the east half of the cofferdam. Additional entrainment from the hypolimnion occurred at the cofferdam where the pumpback jet entrained flow from lower layers. Surface-entrained flow was observed to come from west of the cofferdam. Approximately 80 percent of the entrained volume was supplied by the hypolimnion with the remaining 20 percent from the epilimnion. Total entrainment was 1.6 times the pumpback volume.

Option C

28. Pumpback flow for this design was similar to Option B with one exception. Much of the flow entrained from the hypolimnion passed through the breach in the east end of the cofferdam which formed strong

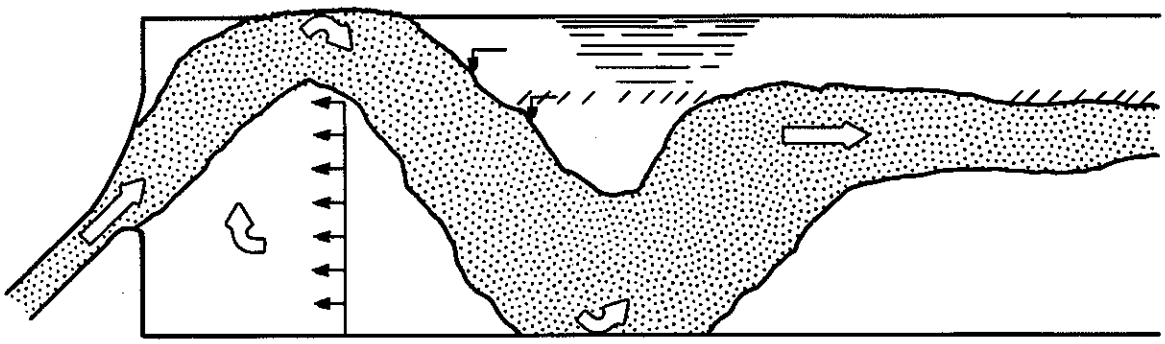

a. OPTION A

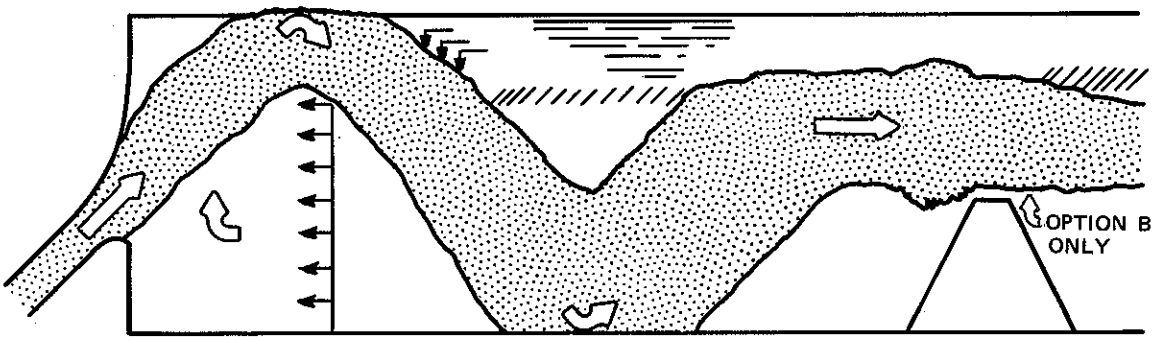

b. OPTION B AND C

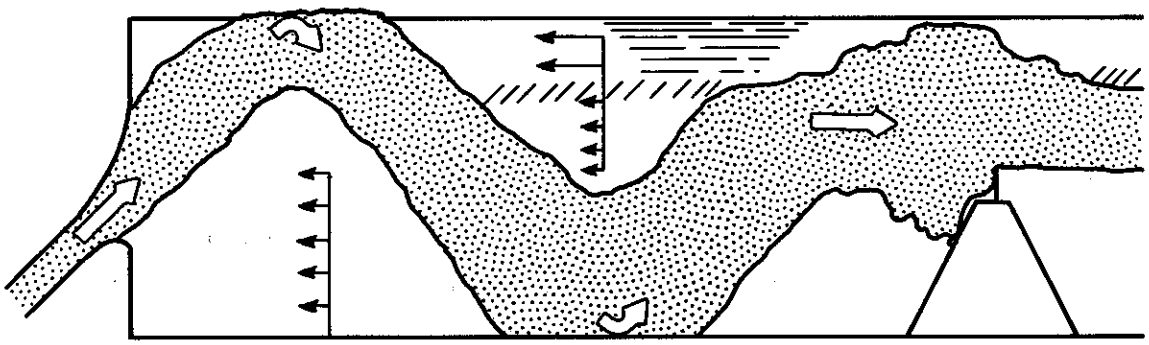

c. OPTION D

Figure B4. A schematic of the pumpback jet flow pattern for each option investigated

lateral currents on the upstream face of the cofferdam. As a result, little or no entrainment occurred as this pumpback jet passed over the cofferdam. Total entrainment for this design is 1.5 times the pumpback volume with the same distribution as in Option B.

Option D

29. The pumpback flow for Option D was significantly different from Options A, B, and C. The elevated cofferdam deflected approximately 40 percent of the pumpback flow along the south side of the cofferdam and inhibited entrainment from the hypolimnion. In addition, the pumpback jet was significantly weakened prior to crossing the cofferdam, resulting in a pumpback flow that crossed the cofferdam as a density current with a lower boundary at el 400.

30. Entrainment was primarily from the epilimnion (85 percent) and was from west of the cofferdam. Approximately 10 percent of the entrainment was from the hypolimnion above el 400 and the remaining 5 percent from below el 400. Total entrainment was 1.0 times the pumpback volume.

In accordance with letter from DAEN-RDC, DAEN-ASI dated 22 July 1977, Subject: Facsimile Catalog Cards for Laboratory Technical Publications, a facsimile catalog card in Library of Congress MARC format is reproduced below.

Evaluation of in-reservoir cofferdam on Richard B. Russell Reservoir and hydropower releases : hybrid model investigation / by Dennis R. Smith ... [et al.] (Hydraulics Laboratory, U.S. Army Engineer Waterways Experiment Station). -- Vicksburg, Miss. : The Station ; Springfield, Va. : available from NTIS, 1981.
55 p. in various pagings : ill. ; 27 cm. -- (Technical report / U.S. Army Engineer Waterways Experiment Station ; HL-81-12)
Cover title.
"October 1981."
"Prepared for U.S. Army Engineer District, Savannah."
Includes bibliographies.

1. Hydrodynamics. 2. Mathematical models. 3. Richard B. Russell Reservoir (Georgia and South Carolina).

Evaluation of in-reservoir cofferdam : ... 1981.
(Card 2)

4. Water--Dissolved oxygen. I. United States. Army. Corps of Engineers. Savannah District. II. U.S. Army Engineer Waterways Experiment Station. Hydraulics Laboratory. III. Series: Technical report (U.S. Army Engineer Waterways Experiment Station) ; HL-81-12.
TA7.W34 no.HL-81-12